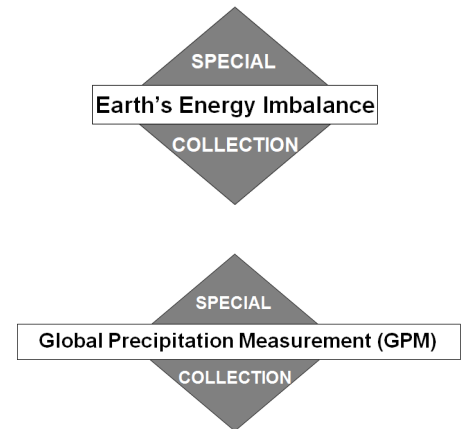


Closing the Water Cycle from Observations across Scales

Where Do We Stand?

Wouter Dorigo, Stephan Dietrich, Filipe Aires, Luca Brocca, Sarah Carter, Jean-François Cretau, David Dunkerley, Hiroyuki Enomoto, René Forsberg, Andreas Güntner, Michaela I. Hegglin, Rainer Hollmann, Dale F. Hurst, Johnny A. Johannessen, Christian Kummerow, Tong Lee, Kari Luojus, Ulrich Looser, Diego G. Miralles, Victor Pellet, Thomas Recknagel, Claudia Ruz Vargas, Udo Schneider, Philippe Schoeneich, Marc Schröder, Nigel Tapper, Valery Vuglinsky, Wolfgang Wagner, Lisan Yu, Luca Zappa, Michael Zemp, and Valentin Aich



ABSTRACT: Life on Earth vitally depends on the availability of water. Human pressure on fresh-water resources is increasing, as is human exposure to weather-related extremes (droughts, storms, floods) caused by climate change. Understanding these changes is pivotal for developing mitigation and adaptation strategies. The Global Climate Observing System (GCOS) defines a suite of essential climate variables (ECVs), many related to the water cycle, required to systematically monitor Earth’s climate system. Since long-term observations of these ECVs are derived from different observation techniques, platforms, instruments, and retrieval algorithms, they often lack the accuracy, completeness, and resolution, to consistently characterize water cycle variability at multiple spatial and temporal scales. Here, we review the capability of ground-based and remotely sensed observations of water cycle ECVs to consistently observe the hydrological cycle. We evaluate the relevant land, atmosphere, and ocean water storages and the fluxes between them, including anthropogenic water use. Particularly, we assess how well they close on multiple temporal and spatial scales. On this basis, we discuss gaps in observation systems and formulate guidelines for future water cycle observation strategies. We conclude that, while long-term water cycle monitoring has greatly advanced in the past, many observational gaps still need to be overcome to close the water budget and enable a comprehensive and consistent assessment across scales. Trends in water cycle components can only be observed with great uncertainty, mainly due to insufficient length and homogeneity. An advanced closure of the water cycle requires improved model–data synthesis capabilities, particularly at regional to local scales.

KEYWORDS: Hydrologic cycle; Satellite observations; Surface fluxes; Surface observations; Water masses/storage; Water budget/balance

<https://doi.org/10.1175/BAMS-D-19-0316.1>

Corresponding authors: Wouter Dorigo, wouter.dorigo@geo.tuwien.ac.at; Stephan Dietrich, dietrich@bafg.de

In final form 30 March 2021

©2021 American Meteorological Society

For information regarding reuse of this content and general copyright information, consult the [AMS Copyright Policy](#).

AFFILIATIONS: **Dorigo, Wagner, and Zappa**—Department of Geodesy and Geoinformation, TU Wien, Vienna, Austria; **Dietrich**—International Centre for Water Resources and Global Change, German Federal Institute of Hydrology, Koblenz, Germany; **Aires**—LERMA, CNRS/Observatoire de Paris, Paris, France; **Brocca**—Research Institute for Geo-Hydrological Protection, National Research Council, Perugia, Italy; **Carter**—Laboratory of Geo-Information Science and Remote Sensing, Wageningen University and Research, Wageningen, Netherlands; **Cretau**—Laboratoire d'Études en Géophysique et Océanographie Spatiales, Toulouse, France; **Dunkerley and Tapper**—School of Earth, Atmosphere and Environment, Monash University, Melbourne, Victoria, Australia; **Enomoto**—National Institute of Polar Research, Tokyo, Japan; **Forsberg**—National Space Institute, Technical University of Denmark, Kongens Lyngby, Denmark; **Güntner**—Helmholtz Centre Potsdam GFZ German Research Centre for Geosciences, and Institute of Environmental Science and Geography, University of Potsdam, Potsdam, Germany; **Heggin**—Department of Meteorology, University of Reading, Reading, United Kingdom; **Hollmann and Schröder**—Satellite-Based Climate Monitoring, Deutscher Wetterdienst, Offenbach, Germany; **Hurst**—Cooperative Institute for Research in Environmental Sciences, University of Colorado Boulder, and NOAA Global Monitoring Laboratory, Boulder, Colorado; **Johannessen**—Nansen Environmental and Remote Sensing Center, and Geophysical Institute, University of Bergen, Bergen, Norway; **Kummerow**—Department of Atmospheric Science, Colorado State University, Fort Collins, Colorado; **Lee**—Jet Propulsion Laboratory, California Institute of Technology, Pasadena, California; **Luoju**—Finnish Meteorological Institute, Helsinki, Finland; **Looser and Recknagel**—Global Runoff Data Centre, German Federal Institute of Hydrology, Koblenz, Germany; **Miralles**—Hydro-Climate Extremes Lab, Ghent University, Ghent, Belgium; **Pellet**—Institute of Industrial Science, The University of Tokyo, Tokyo, Japan; **Ruz Vargas**—International Groundwater Resources Assessment Centre, Delft, Netherlands; **Schneider**—Global Precipitation Climatology Centre, Deutscher Wetterdienst, Offenbach, Germany; **Schoeneich**—Institute for Urban Planning and Alpine Geography, University Grenoble Alpes, Grenoble, France; **Vuglinsky**—Hydrological Institute, Saint Petersburg, Russia; **Yu**—Physical Oceanographic Department, Woods Hole Oceanographic Institution, Woods Hole, Massachusetts; **Zemp**—University of Zurich, Zurich, Switzerland; **Aich**—Global Climate Observing System, Geneva, Switzerland

Life on Earth is intimately connected to the availability of water, to the point that when we search for life on other planets, we search for water. Its circulation through the hydrological cycle sustains Earth's biosphere, which remains inherently vulnerable to the variability in water supply. With a steadily increasing world population and economic development, the demands on water resources and the potential damage by hydrometeorological extremes like droughts and floods are increasing too. But it is not only the hydrosphere that has impacted us, as vice versa, it is likely that human activities have influenced the global water cycle since the mid-twentieth century (e.g., Bindoff et al. 2013; Marvel et al. 2019; Padrón et al. 2020; Bonfils et al. 2020). However, observational uncertainties in combination with strong natural climate variability render estimates of the human contribution to recent trends uncertain, and overall challenge the detection and attribution of change, in particular with regard to extremes and local phenomena (Hegerl et al. 2015; National Academies of Sciences, Engineering, and Medicine 2016).

The Paris Agreement of the UNFCCC also addresses these observational needs and demands that “Parties should strengthen ... scientific knowledge on climate, including research, systematic observation of the climate system and early warning systems, in a manner that informs climate services and supports decision-making” (United Nations 2015). The call of the UNFCCC for enhancing systematic observations expresses the need for climate monitoring based on best available science, which is globally coordinated through the Global Climate Observing System (GCOS). In the current implementation plan of GCOS, main observation

gaps are addressed and it states that “closing the Earth’s energy balance and the carbon and water cycles ... through observations remain outstanding scientific issues that require high-quality climate records of ECVs” (GCOS 2016). Water-related ECVs are specified by GCOS and critically contribute to the characterization of Earth’s climate including the global water cycle (Bojinski et al. 2014). They are also the focus of the Global Energy and Water Exchanges (GEWEX) program (<https://www.gewex.org>) that seeks to understand the state of the hydrologic cycle and the processes that affect it.

Components of the water cycle. The water cycle, also known as the hydrological cycle, describes the continuous movement of water between storages at, above, and below Earth’s surface. [Figure 1 presents observed estimates of global water cycle storages (in 10^3 km^3) and their uncertainties while Figure 2 presents annual global water cycle fluxes (in 10^3 km^3) and their trends. Sources of individual estimates are reported in Table 1.] We summarize the status and long-term changes trends of both the changes in storage but also changes in fluxes, respectively. Storages include water bodies (oceans, seas, lakes, rivers, artificial reservoirs), atmospheric water (water vapor, clouds), subsurface water (soil moisture, groundwater), frozen water (glaciers, ice sheets, sea ice, snow, ground ice), and the biosphere as a whole. The key fluxes linking these storages include

- terrestrial and surface water evaporation and sublimation;
- precipitation, either in liquid, gas, or frozen state;
- uptake and release by the cryosphere, lakes and artificial reservoirs, and aquifers;
- surface water runoff and flow; and
- recharge and depletion of water bodies by humans.

On a yearly basis, only about 0.008% of the water available on Earth is cycled (Oki and Kanae 2006). In other words, theoretically, it takes about 12,500 years until all water molecules have completed a full ocean–atmosphere–land–ocean cycle.

The largest water cycle fluxes take place over the ocean: The ocean produces about 87% of the global evaporation and receives approximately 78% of the global precipitation

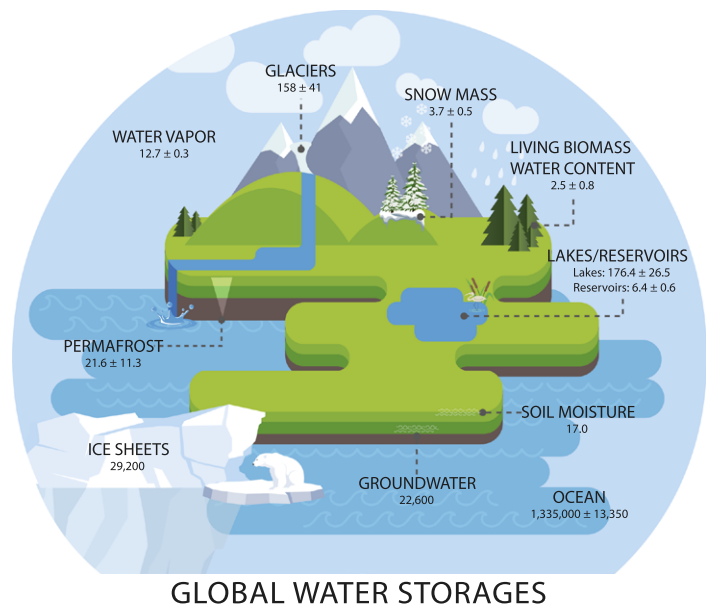


Fig. 1. Observed estimates of global water cycle storages (in 10^3 km^3) and their uncertainties. Sources of individual estimates are reported in Table 1.

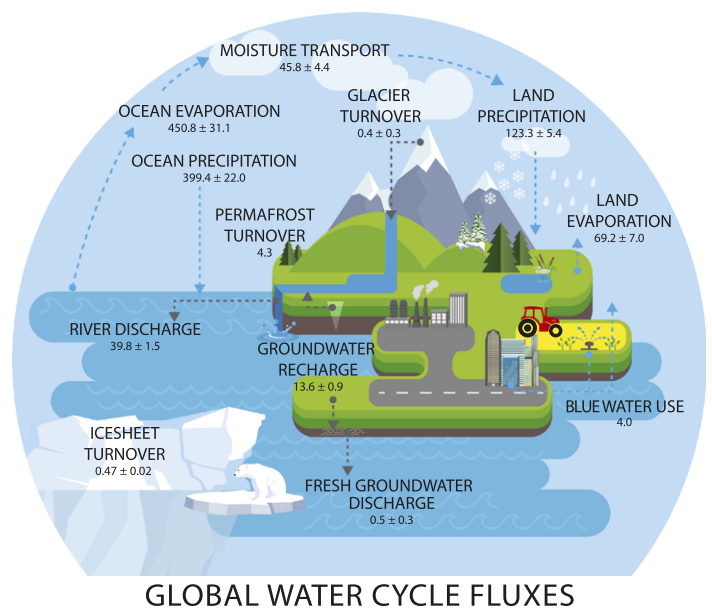


Fig. 2. Observed estimates of annual global water cycle fluxes (in 10^3 km^3) and their trends. Sources of individual estimates are reported in Table 2.

Table 1. Summary of water cycle storages including trends. All values in 10³ km³ (storage) or 10³ km³ yr⁻¹ (trends). Glacier and ice sheets ice weight is calculated to volume by ice density, assuming an ice density of 917 kg m⁻³ (IPCC AR5).

| Stores | Total volume (10 ³ km ³) | Uncertainty (1 sigma) | Uncertainty (%) | Source | Global trends (10 ³ km ³ yr ⁻¹) | Trend uncertainty (95% confidence level) | Source | Type of observation |
|---|---|--|------------------------|---|---|--|---|---|
| Water stored in oceans | 1,335,000.0 | 13,350 | 1% | ngdc.noaa.gov/mgg/global/etopo1_ocean_volumes.html | 1) 391 (1957–2018), 2) 762 (1993–2018), 3) 539–666 (GRACE, 2003–18) | 1) ±95, 2) ±169 | 1), 2) Frederikse et al. (2020), 3) Blazquez et al. (2018) | EO, in situ |
| Water stored in lakes | 176.4 | 26.46 | 15 | Korzoun et al. (1978), Shiklomanov and Rodda (2004) | Not rated | Not rated | Not rated | EO, in situ |
| Water stored in reservoirs | 6.4 | 0.64 | 10 | Shiklomanov (2008) | Not rated | Not rated | Not rated | EO, in situ |
| Groundwater | 1) 23,400, 2) 22,600 | 16,000–30,000 (range based on porosity uncertainty; Gleeson et al. 2016) | 2) 58%–133% | 1) Oki and Kanae, (2006), 2) Gleeson et al. (2016) | 3) 145 (2000–08), 4) 137 (1960–2010) | 3) 39, 4) — | 3) Konikow (2011), 4) de Graaf et al. (2016) | Volume based on global lithology and porosity; trends from EO, in situ and models |
| Soil moisture | 17 | Not rated | Not rated | Oki and Kanae (2006) | Not rated | Not rated | Not rated | Reanalysis |
| Water stored in permafrost a) NH; b) mountain | 1) 20.8, 2) 0.11 | 1) 11.1, 2) 0.02 | 1) 53%, 2) 21% | 1) Zhang et al. (2000), 2) Jones et al. (2018, 2021) (mountain) | Not rated | Not rated | Not rated | In situ, model calculation based on ice content assumptions |
| Water stored in glaciers | 158 (around year 2000) | 41 | 26% | Farinotti et al. (2019; NCEO) | –0.3 (2006–2015) | 0.1 | IPCC (2019), based on Zemp et al. (2019), Wouters et al. (2019), and regional studies | EO, in situ |
| Water stored in ice sheets and ice shelves | 29,200 | Not rated | Not rated | Shepherd et al. (2018) | –0.472 (2006–15) | 0.024 | IPCC (2019), based on Bamber et al. (2018) | EO, in situ |
| Water stored in snow | 3.7 | 0.5 | 3%–4% (mountains ~10%) | Pulliainen et al. (2020) | –0.049 (for 1980–2018) | ±0.049 (95% significance) | Pulliainen et al. (2020) | EO, in situ |
| Water stored in vegetation | 2.46 | 0.82 | Not rated | This study, based on Tong et al. (2020), Spawn et al. (2020), Penman et al. (2003) | Not rated | Not rated | Not rated | EO, in situ |
| Atmospheric water vapor | 12.7 | 0.3 | 2%–3% | Trenberth et al. (2007) | Small positive trend | Medium certainty | Chen and Liu (2016) | EO, in situ, reanalysis |

(Baumgartner and Reichel 1975; Oki and Kanae 2006). The imbalance implies a net moisture transport from the ocean to the continents through the atmosphere, making the ocean an important source of continental precipitation (Trenberth et al. 2011; Gimeno et al. 2012). The net transport of freshwater from the ocean to the continents through the atmosphere is compensated by river discharge. Other runoff sources, such as annual snow and ice melt and groundwater flow into the ocean are estimated to be less than 10% of the river discharge (Burnett et al. 2001).

Human impacts on the water cycle. Nowadays, nearly all components of the water cycle are directly or indirectly influenced by humans (Abbott et al. 2019). Direct anthropogenic impacts include the extraction of ground or surface water for agricultural, domestic, or industrial purposes or the construction of reservoirs. However, indirect changes, caused by human-induced global warming or land use and land cover change, have possibly even further-reaching consequences. Rising temperatures impact the cryosphere by causing the decline of glaciers and ice sheets (Zemp et al. 2019), by shortening the snow-covered season in alpine areas and northern latitudes (Pulliainen et al. 2020), and by exacerbating sea ice melt. The resulting changes in albedo have shown to lead to more stable weather patterns, thus influencing the distribution of precipitation in space and time (Doughty et al. 2012). At a more local scale, a change to more rain and less snow in montane catchments in a warmer future may have severe implications for seasonal water availability (e.g., Singh and Bengtsson 2004; Berghuijs et al. 2014). Discharge is expected to peak in some catchments as glacier melt swells rivers before declining as glacier mass reduces in a warming climate (e.g., Pritchard 2019; Allan et al. 2020).

Anthropogenic global warming increases the water holding capacity of the atmosphere, with consequences for evaporation and precipitation patterns over ocean and land (see sidebar). It is expected that in a warmer world extreme precipitation events will deliver a larger proportion of total annual precipitation (Fowler et al. 2021, Pfahl et al. 2017). This may impact many water cycle processes, including increased surface runoff, and more variable rainfall arrival may reduce water security (Eekhout et al. 2018). Simultaneously, an increase in large rainfall events may beneficially enhance groundwater recharge, particularly in dry climates, where major rainfall events are frequently required to trigger groundwater recharge (Thomas et al. 2016). Precipitation is also subject to modification if the condition of the land surface is altered: large-scale loss of tropical forests may cause rainfall change via reduced and seasonally changed plant transpiration and the altered precipitation recycling that can result (Ellison et al. 2017; Peña-Arancibia et al. 2019). Changes in land surface conditions may also affect large-scale temperature gradients and thus circulation and moisture advection (Zhou et al. 2021).

There is also strong evidence of clear links between global warming, evaporative demand, and the promotion of drought and aridity (S. Zhou et al. 2019; Williams et al. 2020; Vicente-Serrano et al. 2020), but the strength of these relationships varies regionally and seasonally (Cook et al. 2020a). Conversely, Cook et al. (2020b) have shown that large-scale expansion and intensification of irrigation has buffered warming trends in some regions, but it is not certain if these trends will persist under future climate change conditions. A reduction in relative humidity over land is a particularly strong climate change signal in both observations and model results and has been clearly linked to warming over neighboring oceans (Byrne and O’Gorman 2016, 2018).

Agricultural production, especially from irrigation as noted above, alters evaporative fluxes from the land surface. The net effect of raising atmospheric CO₂ levels on plant physiology and the water cycle are still uncertain. On the one hand, CO₂ fertilization may cause increased water use efficiency and suppress plant transpiration (Gedney et al. 2006; Berg and Sheffield 2019) resulting in higher maximum daily temperatures (Lemordant and Gentine 2019) with an additional possible feedback to evaporation, but also allows greater retention of soil moisture, and larger runoff ratios during rainfall (e.g., Idso and Brazel 1984; Kooperman et al. 2018). On the other hand, enhanced transpiration losses associated with CO₂-driven greening may lead to reduced streamflow (Ukkola et al. 2016).

Observing the water cycle. Earth’s water cycle is monitored through three pillars—in situ observations, satellite observations, and observation-driven modeling. GCOS has currently

defined a set of 54 ECVs, which are variables that are fundamental for monitoring the state of the climate and from an observational perspective mature enough to provide long-term consistent measurements in a systematic way (Bojinski et al. 2014; GCOS 2016). Especially over land, in situ data provide long-term records of the different components of the water cycle (see appendix A, Tables A1 and A2). Global in situ data centers, often operating under the auspices of UN organizations, collect globally available water data, harmonize them, and make them again publicly available. For some variables (e.g., precipitation and river discharge), time series from in situ observations are long enough (>30 years) to allow for detection of climate trends and variability but for most variables (e.g., evaporation over ocean and land), records are much shorter. Moreover, in situ data are sparse and, depending on the variable and process, representative only for a limited spatial domain. The shorter the time series, the more difficult it becomes to separate climate change signals from natural variability and changes caused by direct human interference in the water cycle.

Over the last four decades, the amount of relevant satellite-derived hydrological

variables has significantly increased (Rast et al. 2014), and programs like ESA's Climate Change Initiative (Hollmann et al. 2013) have promoted the combination of water cycle observations from multiple satellites into long-term Climate Data Records (CDRs) (appendix A, Tables A1, A2). The recent expansion of operational missions (e.g., Copernicus Sentinels,

Salinity as a proxy for the ocean water cycle

Ocean salinity has long been regarded as a potential rain gauge of the ocean water cycle (Elliott 1974). The cycling of the freshwater between evaporation E , precipitation P , and runoff R acts in concert with ocean circulation and mixing, driving the salinity distribution to respond to the balance between E , P , and R . Surface waters are generally saltier in the subtropical regions where E exceeds P , and fresher in the tropical and high-latitude regions where P and/or R exceeds E (Schmitt 1995). As the globe warms, the water holding capacity of the atmosphere increases so that more moisture is evaporated from the ocean to the atmosphere. The increased moisture energizes the moisture transport between regions and amplifies the $P-E$ patterns over the ocean. The rate of increase in ocean evaporation is, however, less than the rate predicted by the Clausius–Clapeyron equation, because the global hydrological cycle is constrained by the surface and atmospheric energy budget (e.g., Held and Soden 2006; Hegerl et al. 2015; Allan et al. 2020). Multidecadal ocean observations showed that mean salinity patterns have amplified, leading to a salinification of the subtropical ocean and freshening of the tropical and high latitude (e.g., Durack and Wijffels 2010). The pattern of change in salinity is consistent with the “dry-gets-drier and wet-gets-wetter” paradigm (Held and Soden 2006), indicating that the oceans hold important insights into the long-term variations of the water cycle and the effects of climate change (Yu et al. 2020). Hence, estimates of the global ocean salt budget change serve as an alternative and independent measure to the change of the freshwater budget in the ocean (Llovel et al. 2019) and is particularly appealing in light of large uncertainties in the present estimates of E , P , and R .

The observed rate of the water cycle intensification inferred from in situ salinity observations is about $8\% \pm 5\% \text{ } ^\circ\text{C}^{-1}$ of global mean surface temperature rise over 1950–2000 (Durack et al. 2012). This rate is in line with theory, but more than twice as large as the rates estimated from state-of-the-art climate models. Several modeling studies have suggested that the disparity may reflect the effects of ocean warming on the surface salinity pattern amplification in addition to the effects of changing $P-E$ flux arising from the strengthening water cycle (Zika et al. 2018). Ocean warming acts to increase near-surface stratification, prolonging existing salinity contrasts and causing surface salinity patterns to amplify further. Changes in atmospheric circulation patterns alter the locations of the wet and dry portions of the atmospheric circulation, which can also dampen the water cycle change signal passed on to the ocean (e.g., Allan et al. 2020). Hence, the use of ocean salinity as a proxy for $P-E$ should be aware that the processes responsible for the change of ocean salinity may not be as straightforward as a simple response to changes in the $P-E$ field.

Advances in L-band (1.4 GHz) microwave satellite radiometry in the recent decades, pioneered by the ESA's SMOS and NASA's Aquarius and SMAP missions, have demonstrated an unprecedented capability to observe global sea surface salinity from space (Vinogradova et al. 2019; Reul et al. 2020). These satellite salinities are complementary to the existing in situ systems such as Argo profiling floats, enabling the salinity observing capability to reach to a depth of 2,000 m. It is hoped that the assimilation of satellite and Argo salinities in ocean state estimation and coupled ocean–atmosphere system will lead to advances in estimating the freshwater budget over the global ocean through enforcing ocean dynamical constraints on the changes of $P-E$ as well as R .

EUMETSAT MetOp, NOAA JPSS) jointly with innovative explorer satellites [e.g., GPM, GRACE(-FO), Aeolus, SMOS, SMAP, SWOT] is improving our observational capacity, while methodological progress such as artificial intelligence reduces retrieval errors and improves uncertainty descriptions. Nonetheless, observing subtle climate change signals like extreme events, and adequately characterizing errors of the observations remains challenging.

Reanalysis systems assimilate a broad array of observations into atmosphere, ocean, and land models to compute a suite of prognostic variables (e.g., Hersbach et al. 2020). Reanalyses are particularly important for studying water cycle variability, since they aim to provide complete and continuous information. However, self-consistency in reanalyses is not guaranteed (Albergel et al. 2013; Trenberth et al. 2011). Issues arise from the heterogeneous mix of assimilated observations (which exhibit varying spatial and temporal representativeness and accuracy), as well as systematic biases in the modeling system itself (Bosilovich et al. 2017). Although the latest generation of reanalysis products, e.g., MERRA-2 or ERA5, show improvements over their predecessors, trends in many of their water cycle components remain uncertain (Bosilovich et al. 2017; Hersbach et al. 2015; Yu et al. 2020). Besides, global-scale changes are particularly difficult to capture in reanalyses since the moisture and energy balances are not constrained. While atmospheric moisture variability has been much improved in the latest generation reanalysis products, global mean changes in precipitation are still not captured. Thus, global-scale water cycle trends in general are unrealistic in reanalysis products (Allan et al. 2020).

Recent state of water budget closure and imbalance. Because of the large variety of observation platforms, methodological approaches, and scientific communities involved, current observed water cycle ECVs are in imbalance, meaning that when adding up all components, water is added to or removed from the global cycle (Sheffield et al. 2009; Luo et al. 2021; Abolafia-Rosenzweig et al. 2021). Popp et al. (2020) proposed a set of rules to improve consistency between CDRs but further research and development, e.g., on ECV interdependencies at the retrieval and scientific levels, is needed to achieve this goal for observed water cycle components. There is also the problem of missing variables pertinent to the closure of the water cycle that cannot be readily observed but have to be obtained from observation-driven modeling, e.g., atmospheric water vapor transport from ocean to land, infiltration.

Based on the state of the art of existing datasets and challenges ahead, GCOS defined observation targets for each individual ECV and for closing the water cycle including associated uncertainty estimates on annual time scales (GCOS 2016). The GCOS target for closing the global water cycle is within 5% annually, but without being backed up by a solid argument. In theory, the CDRs currently available should be sufficient to achieve this target and, indeed, in the majority of cases, the observed annual surface and atmospheric water budgets over the continents and oceans close with much less than 10% residual (GCOS 2015). Posing additional closure constraints allows to further reduce the errors of the individual variables (Pellet et al. 2019).

Even if annual closure within 5% uncertainty can be attained, this does not necessarily allow for monitoring water cycle variability in all its facets. Appropriate climate monitoring also requires consistency at subannual time scales (e.g., seasonal, monthly, or shorter) to monitor changes in extremes like storms, floods, heatwaves, and droughts (Koutsoyiannis 2020). For these time scales, observed residuals and optimized uncertainty estimates are considerably larger, often nearing or exceeding 20% (Rodell et al. 2015). Moreover, even at the time scale of only a few decades average storages and fluxes are not static, since human-induced global warming and direct intervention in the Earth system have substantial impact on each of the terms (Wada et al. 2012). Thus, apart from water cycle closure at short time scales, also the sum

of all trends needs to close (e.g., Stephens et al. 2012; Allan et al. 2020; Gutenstein et al. 2021; Thomas et al. 2020)

The goal of this paper is to provide a holistic review of available global long-term land, atmosphere, and ocean water cycle storage (second section 2) and flux (third section) products from in situ and Earth observations. Reanalysis data are only discussed if direct observations are impossible. In particular, supported by a review on existing water cycle closure studies, we evaluate how well these products perform in closing the water cycle at multiple temporal (annual, monthly, multidecadal) and spatial (global, basin, pixel) scales (fourth section). Based on the review, we discuss gaps in existing observation systems and formulate guidelines for future water cycle observation strategies for implementation in GCOS (fifth section). While in the second and third sections we focus on the storages and fluxes one by one, we synthesize the common benefits, limitations, or difficulties in the fifth section. A list of terms and definitions can be found in appendix B.

Observing water cycle storages

Ocean (fresh)water storage. Oceans contain 96.5% of the water on Earth (Eakins and Sharman 2010), taking into account water volume in the upper 2 km of Earth's crust. Observations of global mean sea level (GMSL) can be used to infer the change of ocean freshwater storage after removing the effect of thermal expansion and glacial isostatic adjustment.

Tide gauge networks date back to the late nineteenth century and are sparsely distributed along the coasts, which is a major factor contributing to the uncertainty of the estimated change of GMSL. Historical ocean temperature measurements have been used to estimate the thermal expansion of the global ocean through time (e.g., Levitus et al. 2012; Ishii et al. 2017), however, much of the historical ocean temperature measurements had been in the upper few hundred meters and sparsely distributed along ship tracks. The development of the Argo profiling floats since the mid-2000s have enabled a near-global array of Argo floats that sample the ocean down to a depth of 2,000 m. Full-depth Argo floats are being developed, complementing the full-depth shipboard hydrographic measurements from research vessels.

Satellite altimeters have revolutionized the study of GMSL change by providing full global coverage since the 1990s. Satellite measurements from GRACE(-FO) have provided reliable estimates of the change of global ocean mass from 2003 onward, although this record is likely too short to characterize the long-term trend (Blazquez et al. 2018).

Lakes and artificial reservoirs. Lakes range in size from small ponds to inland seas. Their geographical distribution is very irregular, while most are located at high latitudes in formerly glaciated areas of the Northern Hemisphere (Downing et al. 2006; Williamson et al. 2009). Reservoirs are water bodies with artificial regulation of water reserves. Most reservoirs are constructed for hydropower purposes, but smaller ones exist for irrigation purposes.

Water volume (change) is estimated from water level observations using a so-called volume curve, which describes the relationship between water level and the corresponding water volumes based on the lake's or reservoir's morphology. For many large lakes, such volume curves are available but need to be regularly updated due to changes in the morphometric characteristics over time. For reservoirs, these curves are computed in the design phase and regularly updated in connection with the sedimentation of reservoirs. In situ observations of lake water level are usually carried out by national hydrological networks, adopting the standards prescribed by WMO. Thus, most in situ observations of lake water level are globally consistent and have accuracies of ± 1 cm (WMO 2008). Long-term sampling efforts have primarily focused on northern temperate sites, while observations are scarce in many other areas, including remote, lake-rich regions in the Canadian and Siberian (sub-)

Arctic, less-populated areas like the Himalayas and the Andes, and populated regions like the African Great Lakes.

Despite being less accurate than in situ observations, current satellite altimeters provide dense measurement time series of water surface elevation for the largest lakes, and optical and radar observations of lake area. Water volume (change) of a large number of lakes can thus be inferred from the combination of satellite observations of water level and extent (Gao et al. 2012; Busker et al. 2019; Crétau et al. 2016). Water height and extent observations collected at different epochs can be used to build hypsometry relationships between height and volume changes in order to obtain water volume variations from water heights measured by satellite altimetry (Crétau et al. 2016).

Atmospheric moisture. The atmosphere is one of the smallest storages for water within the water cycle (Trenberth et al. 2007; Gleick 1996). Regionally, seasonal and interannual variations in atmospheric moisture are driven by changes in the distribution of sources (evaporation), sinks (precipitation), and the moisture flux convergence (e.g., Oki 1999). Under steady-state assumptions, the large sources and sinks lead to a short (8.9 ± 0.4 days) global average residence time for atmospheric water (van der Ent and Tuinenburg 2017). Yet despite the small storage capacity of the atmosphere, atmospheric transport is the rate-limiting step in moving water “upstream” from oceans to land. It is noteworthy that this transport constitutes only 10% of the oceanic evaporation source.

Atmospheric moisture is measured by a wide variety of ground-based, balloon- and aircraftborne, and satellite instruments. A near-global network of sites launching balloonborne radiosondes has provided high-resolution vertical profiles of relative humidity (RH) since the mid-1940s (Stickler et al. 2010), but only a few stations provide reliable long-term records for climate trend analysis (Wang and Zhang 2008; Ferreira et al. 2019). Balloonborne frost point hygrometers provide high-resolution, high-quality profiles of water vapor number density up to the middle stratosphere, but soundings are sparse in space and time. Ground-based microwave radiometers, lidars, FTIRs, and GPS receivers provide coarser resolution profiles. Routine, high-quality RH measurements are made from commercial aircraft (Brenninkmeijer et al. 2007; Petzold et al. 2015; Moninger et al. 2010).

Satellite observations of atmospheric moisture (Schröder et al. 2016; Hegglin et al. 2013; Willett et al. 2020) offer near-global coverage, show steady quality and coverage improvements since the late 1970s, and are the main source of measurements over the oceans and developing countries where high-quality in situ measurements are scarce. Nadir-viewing sensors can provide coarse-resolution vertical profiles (e.g., Schröder et al. 2016). Limb-viewing sensors have higher vertical resolution, but are limited mostly to measurements above the middle troposphere (e.g., Hegglin et al. 2013). Nadir-viewing satellite microwave instruments have provided TCWV retrievals, mostly over oceans, since the late 1980s. The SSM/I-based data records exhibit consistent results in tracking changes in precipitable water vapor over the ice-free ocean (e.g., Schröder et al. 2016) and, when combined with ERA5 over remaining regions, can be used to analyze global trends (e.g., Allan et al. 2020).

Nadir-viewing infrared sounders date back to the early 1980s (radiometers) and 2000s (spectrometers with higher accuracy and vertical resolution). Infrared instruments measure over both ocean and land but are limited to (near-)clear-sky views, while near-infrared retrievals are limited to over-land and clear-sky views. Finally, high-accuracy GPS radio-occultation profile measurements are routinely made in all weather conditions since 2001 (Wickert et al. 2001).

Soil moisture. Soil moisture strongly interacts with highly dynamic major water and energy fluxes, importantly precipitation, evaporation, and runoff. Therefore, observing systems must

be capable of capturing soil moisture dynamics at their native process scales, which is from subdaily to 10-day time steps, and from tens of meters to tens of kilometers, depending on the considered soil depth and climatic process studied.

The first systematic soil moisture measurements were taken in the 1950s in the former Soviet Union (Robock et al. 2000). Today, many countries, organizations, and individual scientists freely share their in situ soil moisture measurements, most importantly via the International Soil Moisture Network (Dorigo et al. 2021, 2013). Yet most stations are in economically developed regions with temperate climatic conditions and have limited temporal coverage (most stations were established after 2000). Besides, nearly all networks have their unique purpose, design, measurement setup, and representativeness errors, which complicates their use to predict soil moisture at larger scales (Gruber et al. 2013; Dorigo et al. 2021).

Microwave remote sensing satellites have provided a growing number of global soil moisture datasets since the beginning of this century. Global soil moisture datasets are operationally provided for several passive and active microwave missions (Entekhabi et al. 2010; Kerr et al. 2012; Wagner et al. 2013) and many of them are fused into global long-term (Gruber et al. 2019; Dorigo et al. 2017) or near-real-time (Yin et al. 2019) multisatellite products. The spatial resolution of these soil moisture datasets ranges between 10 and 50 km, and the temporal sampling is 1–3 days. The native satellite soil moisture products can only provide information about the soil moisture conditions in the top few centimeters of the soil, but model–data integration and infiltration models can be used to estimate the water content in the root zone (Ford et al. 2014; Babaeian et al. 2019). Estimates of deeper soil layers remain unobserved while their skill reduces for dense vegetation (Dorigo et al. 2010). Although in many areas satellite soil moisture observations are still outperformed by reanalysis products, they start to converge and, in many areas, provide complementary skill (Beck et al. 2021; Dorigo et al. 2017).

Groundwater. Groundwater is by far Earth’s largest liquid freshwater storage (Gleeson et al. 2016), and supports about one-third of human water use (Wada et al. 2014). Its widespread nonsustainable use has led to a depletion of aquifers in many regions worldwide (Famiglietti 2014).

Traditionally, groundwater level is monitored by in situ observations in boreholes or wells and many countries operate a national groundwater monitoring network. (e.g., Hosseini and Kerachian 2017). As setting up and maintaining the networks is costly, groundwater records are often sparse, short, or discontinuous and thus poorly suitable for climate studies. This is further complicated for observations in confined aquifers or those affected by human withdrawals, and by restrictive data sharing policies. The latter also hampers initiatives to combine observations to provide an overview of changes in groundwater levels at a global scale, such as pursued by the Global Groundwater Monitoring Network. Converting the observed head variations into regional groundwater storage variations involves considerable uncertainty from poorly known storage coefficients or specific yield values (Chen et al. 2016), site-specific dynamics (Heudorfer et al. 2019), or management-driven clustering of observation wells in highly productive aquifers while neglecting others.

Since April 2002, GRACE and GRACE-FO provide estimates of Earth’s variations of total terrestrial water storage (TWS) with at least monthly resolution. After removing from TWS the signal components that are not due to groundwater (i.e., soil moisture, surface waters, snow, and ice), it allows for monitoring groundwater storage dynamics (e.g., Rodell et al. 2018). Limitations of satellite gravimetry for monitoring groundwater dynamics are its coarse spatial resolution (>200 km), the necessary filtering of the raw data to remove noise at the expense of attenuation and spatial smoothing (leakage), and the uncertainties in usually model-based estimates of other mass variations (Chen et al. 2016).

Beyond recent progress with dynamic, gradient-based groundwater models at the global scale (de Graaf et al. 2015; Reinecke et al. 2019), there have been numerous developments on assimilating GRACE-based TWS into land surface and hydrological models with simple groundwater schemes. This allows for separating TWS into its compartments for individual river basins and aquifers, and recently also globally (Li et al. 2019). Results tend to indicate that GRACE data assimilation improves the simulation of groundwater storage variations as long as human groundwater withdrawal schemes are part of the model structure.

Permafrost and ground ice. Permafrost is defined as subsurface material with temperatures constantly below 0°C. Relevant for the water cycle is the so-called ice-rich permafrost, which covers huge areas in Arctic countries and the Tibetan Plateau. Ice-rich permafrost in mountain areas is mostly found in frozen scree slopes, rock glaciers and relict ice bodies. Most of the ground ice is perennial, but the upper decimeters to meters are subject to seasonal thaw and refreeze cycles, thus playing a role in the yearly water cycle. Likewise, the permanent melting of permafrost due to global warming adds water to the transient part of the water cycle.

Permafrost cannot be directly mapped and its distribution, ice richness, and volumes are extrapolated from available ground borehole observations using models. The most up-to-date estimates of the total amount of ice stored in Northern Hemispheric permafrost stem from Zhang et al. (2000, 1999), and are based on the *circum-Arctic map of permafrost and ground ice conditions* (Brown et al. 2002; Heginbottom et al. 1993), with assumptions on total area, thickness, and mean ice-content. Permafrost is present also in ice-free areas of Antarctica, but there is no available estimation of its ice volume.

Ice content of permafrost in rock glaciers is usually estimated through geophysical methods, but more precise quantification can only be achieved by boreholes. Due to large costs and logistical and technical difficulties these are extremely rare. A global estimation of ice content in rock glaciers was achieved from a rock glacier inventory and the use of a standard area/thickness relationship and assumptions on the ice content (Jones et al. 2018). This does not include dead ice bodies from glacial origin that can remain over centuries or millennia in periglacial conditions, and which are considered neither in glacier nor in rock glacier inventories.

Changes in permafrost water storage are due essentially to the deepening of the active layer, which induces melting of ice at the top of the perennially frozen ground and its restitution to the water cycle. Observations of the active layer thickness only partly account for ice volume loss, as land surface subsidence (remotely sensed with ground validation) need to be considered too (Jones et al. 2018, 2021).

Snow. Terrestrial snow is characterized by high spatial and temporal variability and until very recently, snow has been one of the more uncertain components of the water cycle, particularly in mountain areas (Lievens et al. 2019).

Various terrestrial snow parameters have been measured using conventional means for centuries. Snow depth observations are performed at most weather stations in cold climates. Accurate snow mass information can be derived from surface observations of snow depth and SWE for regions and time periods with a sufficiently dense observing network (Brown and Derksen 2013) but there remain vast alpine and high latitude regions with insufficient coverage by conventional observing networks (Brown et al. 2019). SWE is further measured in fixed pointwise locations using snow scales and microwave instruments. Ground-based snow measurements are severely limited by a lack of confidence in how they capture the variability in conditions across larger scales, particularly for heterogeneous landscapes. An improvement to pointwise observations are multiple in situ snow courses along a predefined transect. These are available from several national and regional agencies

(Haberkorn 2019) and provide more representative estimates on a regional scale. The amount of snow course data is, however, even more limited in time and space; thus, they are more often used as reference data.

Regional to hemispheric estimation of SWE and snow mass has been obtained since the 1980s from standalone passive microwave observations (e.g., Chang et al. 1990; Kelly et al. 2003) or from synergistic approaches combining satellite observations with ground data (Pulliainen 2006; Takala et al. 2011, 2017). Standalone passive microwave approaches are somewhat limited in their applicability for hemispheric monitoring, but in combination with in situ data perform similar to reanalysis datasets (Mortimer et al. 2020). Both EO- and model-based approaches can be further improved using appropriate bias correction techniques (Pulliainen et al. 2020). A key challenge for satellite passive microwave instruments is their coarse spatial resolution, which prohibits their accurate utilization for mountainous regions. There is potential in C-band SAR to provide high-spatial-resolution snow depth information in mountainous areas (Lievens et al. 2019), but these estimates are still somewhat uncertain and only available with relevant coverage since 2014, thus limiting the potential to retrieve time series relevant for climate studies.

Glaciers. At decadal to annual time scales, glaciers act as storages with related changes, while at annual scales, their annual mass turnover corresponds to hydrological fluxes. As such, glaciers contribute to runoff during dry/summer seasons even in years with positive annual mass balances, i.e., annually net increase in storage (Weber et al. 2010; Huss 2011). Glaciers are among the highest-confidence natural indicators of climate change [Global Land Ice Measurements from Space (GLIMS); GLIMS and NSIDC 2005; Paul et al. 2009; Bojinski et al. 2014; RGI 2017]. Water storage in glaciers cannot be directly measured but is assessed from inventories of glacier surface area and glacier thickness estimates. Glacier inventories are compiled at national to regional levels mainly based on optical images from air and spaceborne sensors (Paul et al. 2009). Glacier ice thickness observations from field and airborne surveys (Gärtner-Roer et al. 2014; Welty et al. 2020) are used to calibrate analytical and numerical models to estimate the regional and global storage of glacier ice (Farinotti et al. 2019).

Glacier mass changes have been measured in situ with seasonal to annual resolution at a few hundred glaciers worldwide, with a few observation series reaching back to the early twentieth century (Zemp et al. 2015). Decadal glacier elevation and volume changes are assessed from topographic surveys and differencing of related maps and digital elevation models (Zemp et al. 2015), using density assumptions (Huss 2013) for conversion to glacier mass changes. Such geodetic mass changes are available for several glaciers from terrestrial surveys back to the late nineteenth century, for several hundred glaciers from aerial and early spaceborne surveys back to the mid-twentieth century, and potentially for all glaciers from spaceborne surveys since the beginning of the twenty-first century (Zemp et al. 2020, 2019). For data-scarce regions, these results have been complemented with regional glacier change estimates based on satellite altimetry and gravimetry (Moholdt et al. 2012; Bolch et al. 2013; Treichler and Kääb 2016; Gardner et al. 2013; Wouters et al. 2019).

Ice sheets. Ice sheets are defined as ice volumes covering an area of continental size. Only the Antarctic and Greenland ice sheets comply with this definition, with Antarctica often subdivided into the West and East Antarctic ice sheets. By definition, ice sheets only concern the grounded part; the floating parts are attributed to the ice shelf, the melt of which does not change the sea level (Cogley et al. 2011).

The water stored in ice sheets is estimated from ice sheet volume measurements, which are derived by combining airborne radar measurements to define the bottom boundary of the ice

and surface height measurements made by airborne and satellite laser and altimeters. Both Greenland and Antarctica have been almost completely covered in this way. Changes in ice mass can be determined in various ways: by elevation change measurements from satellite altimetry, combined with models of snow density and firn compaction; by estimating changes in mass flux across the grounding lines, using ice velocities from radar interferometry combined with meteorological observations and atmospheric reanalysis of interior precipitation, and climate-firn models; and most reliably by satellite gravity measurements of GRACE/GRACE-FO. Uncertainties in global isostatic adjustments is a major error source in mass change estimates, with uncertainties up to 30% in Antarctica and 5%–10% in Greenland (Shepherd et al. 2018).

Water stored in living biomass. About 40%–80% of the world's terrestrial vegetation is composed of water, but this fraction may strongly vary between species, seasons, and meteorological conditions (e.g., Yebra et al. 2018). The remaining fraction is referred to as living (dry) biomass, which can be divided into the two main components above-ground biomass (AGB)—including living stems, branches, leaves, and fruits—and below-ground biomass (BGB), commonly defined as living root biomass (Penman et al. 2003). The ratio of below- and above-ground biomass (known as root:shoot ratio) is between 0.2 and 0.4 for most forest ecosystems but may vary considerably across biomes and vegetation types, ranging from 0.1 in some forest types to 26 in a cool temperate grassland (Mokany et al. 2006).

While vegetation water content has frequently been estimated from optical remote sensing observations at the local scale (e.g., Dorigo et al. 2009), only very few studies attempted to estimate it for larger spatial domains (e.g., Yebra et al. 2018). On the other hand, microwave observations have a very high sensitivity to the water stored in above-ground vegetation (Jackson and Schmugge 1991). Datasets of microwave VOD, which describes the attenuation of microwave radiance by vegetation, have been developed for various sensors, even over multidecadal time scales (e.g., Moesinger et al. 2020), and related to total vegetation water content (Konings and Momen 2018).

Alternatively, vegetation water content can potentially be estimated from EO-derived AGB and extended to total biomass (AGB+BGB) by applying a plant-specific root:shoot ratio. By applying a multiplication factor based on the characteristic plant-specific relative water content, the total biomass can be used to estimate the total water stored in the vegetation (Yebra et al. 2018). Both optical and radar data can be useful for biomass measurements, but commonly SAR and lidar data are used in combination (e.g., Asner et al. 2012; Mitchell et al. 2017). EO-based AGB estimates need ancillary data, e.g., ground data and close-range remote sensing sources such as terrestrial and airborne lidar data for the calibration and validation of the satellite observations (Herold et al. 2019).

Large uncertainties in global estimates of water stored in biomass result from various measurement errors and generalization throughout the computation chain and from the uneven distribution and quality of in situ data. Additionally, uncertainty information associated with the ground data are often not available. Current biomass mapping from space is hindered by its disconnection from plot-based national forest inventory efforts (Böttcher et al. 2017), and varying definitions used for the source data, and methods used to construct the maps (Herold et al. 2019). Remote sensing signals can also saturate at high biomass values, making mapping in natural and tropical forests particularly uncertain (Avitabile et al. 2016).

Observing water cycle fluxes

Ocean evaporation. With a share of 86% to total global evaporation, evaporation from the oceans dominates the surface-to-atmosphere flux of the water cycle. Direct measurements of ocean evaporation through the eddy-covariance method are currently limited to selected locations with limited duration due to technical challenges in operating the instruments from

mobile platforms at sea (Edson et al. 1998; Landwehr et al. 2015). Evaporation cannot be directly observed from satellites because it does not emit, reflect, or absorb electromagnetic radiation. Evaporation is therefore commonly estimated by parameterizing ocean evaporation process models with surface meteorological variables that can be observed (Liu et al. 1979; Fairall et al. 2003). The required variables are SST, wind speed, near-surface air temperature, and humidity, which can be measured from in situ platforms, including voluntary observing ships (VOS), research cruises, and moored buoys, or derived from optical and/or microwave satellites. VOS observations have a rich history before satellites became available (e.g., Josey et al. 1999). The VOS provide direct observations for all variables required to estimate the moisture flux at the ocean surface, but the observations are spatiotemporally inhomogeneous and clustered over the major shipping lanes. However, in densely sampled regions such as the North Atlantic, the VOS-based flux estimates with a multidecade span are a valuable in situ climatology (Berry and Kent 2011).

Not all variables can be directly retrieved from satellites. SST and wind speed have a relatively direct relationship to the radiance measured by the satellites, whereas air temperature and humidity have to be derived indirectly because the electromagnetic signal is emitted from relatively thick integrated atmospheric layers. Retrieval algorithms are fully empirical and require ancillary data from, e.g., ships and buoys. Presently, the accuracy of derived air temperature and humidity stands as the main source of uncertainty in satellite-based ocean flux products (e.g., Prytherch et al. 2015; Liman et al. 2018), but recent technological advances hold great promise in reducing the uncertainties input variables (e.g., Gentemann et al. 2020).

Reanalysis products have also been used to estimate ocean evaporation (directly related to latent heat flux), but their fidelities are affected by the uncertainties and coverage of the satellite observations assimilated (e.g., Yu et al. 2017; Robertson et al. 2020). Changes in ocean salinity (see sidebar) offer a proxy for inferring ocean evaporation in regions where evaporation dominates over precipitation such as subtropical high-salinity regimes (e.g., Yu et al. 2020). However, the contributions of ocean dynamics need to be accounted for.

Land evaporation. Corresponding to approximately two-thirds of the precipitation falling over the continents, terrestrial evaporation is the second largest hydrological flux over land (Gimeno et al. 2010; Miralles et al. 2011). Its fast response to radiative forcing makes evaporation an early diagnostic of changes in climate, while its pivotal influence on land–atmosphere interactions leads to either amplification or dampening of weather extremes such as droughts or heatwaves (Miralles et al. 2019; Seneviratne et al. 2010).

Today, terrestrial evaporation remains one of the most uncertain and elusive components of Earth’s water balance: it cannot be observed directly from space, and it is only seldom measured in the field through the eddy-covariance method, which often have limited spatial representativeness, particularly over heterogeneous landscapes (Miralles et al. 2011; Fisher et al. 2017).

A range of datasets have been proposed that indirectly derive evaporation from models that combine satellite-observed environmental and climatic drivers of the flux (Fisher et al. 2017; McCabe et al. 2019; Jung et al. 2019). These datasets largely rely on multiple sensors from the *Aqua* and *Terra* platforms, and some long records also include data from earlier optical (e.g., AVHRR) and microwave (SSM/I, SMMR) sensors or use satellite soil moisture data in their retrievals (e.g., Martens et al. 2017). Several studies brought to light strong discrepancies among widely used observation-based global land evaporation datasets (e.g., Talsma et al. 2018; Miralles et al. 2016; McCabe et al. 2016). Current global datasets share (i) systematic errors in semiarid regimes and tropical forests, (ii) an imperfect representation of water stress and canopy interception, and (iii) a poorly constrained partitioning of terrestrial evaporation into its different components (transpiration, interception loss, bare soil evaporation, snow

sublimation, and open water evaporation). Few algorithms to compute transpiration include the effect of CO₂ fertilization processes on water use efficiency explicitly, which can be crucial to address long-term trends (Miralles et al. 2016). Nonetheless, these satellite-based datasets of land evaporation are still used as reference for a wide range of climatic applications, even though recent reanalysis datasets (such as ERA5) show clear improvements with respect to their predecessors (Martens et al. 2018).

Precipitation over ocean and land. Precipitation, both liquid (rainfall) and frozen (snowfall), is spatially very inhomogeneous and can vary rapidly in places with mechanical lifting such as mountains or coastlines. There is also significant diurnal variability with the peak of land precipitation occurring in the late afternoon and early evening, posing high demands on the observation systems.

Precipitation over land is measured quite well by the dense networks of rain gauges operated by many countries. The number of rain gauges operated around the world is roughly 200,000 (Kidd et al. 2017), many of which have been used to produce global gridded products (Schneider et al. 2014; Harris et al. 2014). Rain gauge measurements are influenced by systematic gauge measuring errors, mainly caused by wind effects on precipitation, which is particularly large for snowfall. The interpolated gridded rain gauge measurements have substantial uncertainty and sampling errors over complex terrain or in poorly sampled regions.

Several countries also operate operational radar networks, e.g., the United States, Europe, and Japan (J. Zhang et al. 2016; Makihara 1996; Huuskonen et al. 2014). Various attempts to homogenize existing networks have failed thus far, as they all have somewhat different objectives, quality control, and calibration procedures (Saltikoff et al. 2019). Besides, homogenization is hampered by the extremely large data volumes and limited areal coverage. The retrieval of precipitation from satellites remains challenging due to the strong intermittency and variability of precipitation in space and in time, as well as the fundamentally underconstrained nature of precipitation algorithms. Nonetheless, spaceborne radars and radiometers have successfully retrieved precipitation over land (Petersen et al. 2016; Hou et al. 2014) but their sampling remains poor, and accumulations have thus focused on “merged” products constructed with observations from multiple GEO and/or LEO satellites with or without gauge networks to compensate the drawbacks inherent to individual observations. Additionally, recent approaches for improving rainfall accumulations from space have considered the integration with satellite soil moisture products (Massari et al. 2020; Pellarin et al. 2020). Reanalysis datasets that integrate precipitation observations (e.g., ERA5, NCEP–NCAR) could in principle provide more accurate estimates than pure observation-based products but are equally affected by limitations in the coverage of ground observations, inconsistencies between the assimilated datasets, and errors in numerical modeling (Tarek et al. 2020).

Despite being observationally constrained, the multitude of daily precipitation datasets based on rain gauge measurements, remote sensing, and/or reanalyses, have demonstrated a large disparity in the quasi-global land mean of daily precipitation intensity (e.g., Herold et al. 2019). Masunaga et al. (2019) showed a contrast in global mean and extreme precipitation accumulations of satellite–in situ merged products, with stronger differences in their extreme precipitation. Their results also exhibit stronger differences in extreme precipitation over ocean than over land. In general, Alexander et al. (2020) have shown that global observation-based precipitation products have potential for climate-scale analyses of extreme precipitation frequency, duration, and intensity. Specifically, reanalysis products tend to be much more variable than the observation-based products, particularly over the global oceans (Pellet et al. 2019).

Snowfall products are determined much like their rain counterparts but tend to have an added degree of difficulty associated with them. For radars, snow is less reflective than rain

for the same size particles and since snowfall is often lighter than rainfall, echoes are generally much weaker. The GPM radar satellite is only able to detect moderate to heavy snowfall events. *CloudSat*, while more sensitive, is a nadir staring instrument, which limits sampling to only climatological applications. Its W-band radar, while capable of better sampling, is still limited in its ability to uniquely convert echoes into meaningful snowfall rates given the great variability of particle sizes and densities. In mountainous regions, where snow tends to be most important, radar retrievals are further complicated by clutter from nearby mountains. The added complication for passive microwave retrievals is the relative lack of unique scattering signals over already snow-covered ground. The retrieval of orographic snowfall is challenging as this is typically characterized by copious snowfall with little or no deep cloud developments that are key to characterize precipitation events from passive microwave and infrared observations (Shige and Kummerow 2016; Gonzalez et al. 2019).

River discharge. Regular measurements of river water height started long ago, and include well-known examples such as the annual minimum and maximum water levels of the Nile River for the years 622–1922 (Whitcher et al. 2002). Today, in situ systems still offer the most accurate basis for monitoring river discharge (Fekete et al. 2002). The majority of the river flux into the oceans (~70%) is covered by a set of 472 global gauging stations, of which 327 are freely available (Looser et al. 2007) but usually shared only with a substantial delay by the national authorities that control the observations. Consequently, the temporal coverage of the available data is heterogeneous, with the highest number of stations available for the period 1980–2000. Because of the incomplete coverage of observations, estimations of total river discharge into the oceans rely on statistical or model-based extrapolation methods (e.g., Baumgartner and Reichel 1975; Milliman and Farnsworth 2011; Ghiggi et al. 2019).

Remote sensing provides a valuable additional source of flow data for unmonitored or infrequently monitored rivers. Discharge can be estimated using particle image velocimetry and bathymetric lidar, though uncertainties in depth, flow speed, and estimated volumetric flow rates can be large (Huang et al. 2018; Kinzel and Legleiter 2019). Satellite altimetry coupled with satellite imagery and hydrodynamic modeling also offer adequate solutions (Kittel 2020), but uncertainties are large for rivers substantially obscured by riparian forest cover or ice covers and ice jams in winter, causing a seasonal bias with increased uncertainties in the discharge estimates (Hicks and Beltaos 2008). Finally, short-lived flood flows in dryland rivers can be difficult to quantify using remote sensing methods.

Groundwater recharge and discharge. Recharge of groundwater occurs by percolating precipitation and surface water, while losses are due to discharge to continental surface water bodies and to the ocean, evaporation, and groundwater pumping. Groundwater storage typically responds in a delayed and smoothed way to precipitation dynamics while actual residence times of groundwater can vary over several orders of magnitude depending on the climate and hydrogeological conditions and on its depth below the Earth surface (Foster et al. 2013). Groundwater recharge occurs at widely varying rates, which can be modulated by human use of the landscape and land cover change. Groundwater recharge rates may be enhanced by managed aquifer recharge, which is widely used globally and is estimated to contribute ~10 km³ annually to the global groundwater system (~1% of total groundwater extraction) (Stefan and Ansems 2018; Dillon et al. 2019).

Groundwater discharge naturally occurs either as submarine groundwater discharge (SGD) or as groundwater discharge to rivers, lakes, and springs. SGD can be divided in three components: groundwater discharge below sea level (fresh SGD), meteoric groundwater discharge above sea level near the coast [nearshore terrestrial groundwater discharge (NGD)], and recirculated seawater (Luijendijk et al. 2020). Fresh SGD and NGD combined correspond to coastal

groundwater discharge (CGD) (Luijendijk et al. 2020). Total SGD is difficult to quantify due to its spatial and temporal variability (Sadat-Noori et al. 2015; Srinivasamoorthy et al. 2019) and the difficulty to measure it. Available techniques are water budgets, hydrogeological modeling, physical measurements, and the use of geochemical tracers (Srinivasamoorthy et al. 2019). Contrary to river discharge, groundwater discharge is usually not monitored, and there is no global database of SGD data.

Glacier and ice sheet annual turnover. Annual glacier mass turnover can be measured at individual glaciers by the component or flux-divergence approach (Bamber and Rivera 2007). However, at regional to global scale corresponding estimates are only available from modeling studies (Kaser et al. 2010; Braithwaite and Hughes 2020; Huss and Hock 2015). The annual mass turnover can be estimated from the mass-balance amplitude, expressed by half the difference between winter and summer balances. The runoff from snow and glaciers in mountain regions feed rivers and groundwater, while some is evaporated (Goulden and Bales 2014). In the Arctic and Antarctic, glaciers often flow directly into the ocean and lose mass through meltwater discharge and calving of ice (King et al. 2020).

Similarly, the Greenland and Antarctic ice sheets feed large amounts of freshwater to the ocean (Enderlin et al. 2014; IPCC 2019). Although the freshwater supply from ice sheets to the ocean is large, observation gaps cause large uncertainties (IPCC 2019). Ice sheet fluxes to the oceans can be determined from satellite measurements of ice velocities and airborne radar thickness around the perimeter of the ice sheet, with major error source being the unknown depths of key outlet glacier systems, especially in East Antarctica. Freshwater flux estimates based on GRACE or elevation changes from space or airborne laser and radar measurements are similarly inaccurate due to errors in snowfall and firn compaction estimates, and the “steady state” ice sheet velocities. Prior to the satellite era (starting in 1992) the knowledge of ice sheet mass balance is highly uncertain and strongly dependent on model assumptions (Slater et al. 2020).

Anthropogenic water use. According to the review about the human impact of the global water cycle by Abbott et al. (2019) the total human water appropriation is estimated to flux magnitude as large as a quarter of total land precipitation. Freshwater used for irrigation, livestock, and industrial and domestic consumption is primarily extracted from groundwater and surface water bodies and flows (blue water). Irrigation accounts for approximately 70% of anthropogenic freshwater withdrawals worldwide (Foley et al. 2011; Shiklomanov 2000). Since 1958, global statistics on anthropogenic water use have been made available by FAO (FAO 2021). Data are reported by each country as annual volumes with a usual delay of 2–4 years, are globally incomplete, and lack standardization across different countries. Data are therefore of limited use for characterizing water use responses to climate variability at sufficient spatial scale and temporal resolution. Other national and subnational surveys may be available (e.g., Deines et al. 2017), but not only are these datasets uncertain, they are also inadequate because they are spatially and temporally lumped.

Remote sensing has emerged as a promising means to provide spatially and temporally explicit estimates of irrigation water volumes, thus overcoming the above-mentioned limitations. Optical and thermal remote sensing have been used to estimate actual evaporation, which can be coupled to the water/energy balance allowing to estimate irrigation volumes (Droogers et al. 2010; van Dijk et al. 2018; Lopez et al. 2020). Because of its direct relationship with irrigation, soil moisture, globally observed from satellites, is naturally designed to inform about the amount of water entering the soil (Kumar et al. 2015; Brocca et al. 2018; Jalilvand et al. 2019; Zaussinger et al. 2019). However, the coarse spatial resolution (10–40 km) of most soil moisture products represents a major constraint for accurate irrigation retrieval.

Once irrigation volumes are estimated, it would be possible to determine groundwater abstraction rates (e.g., Lopez et al. 2020). Although gravimetry-based remote sensing can inform about changes in TWS globally (Voss et al. 2013; Famiglietti 2014), they do not differentiate between natural and anthropogenic loss, or between the different types of water use. Besides, they are not suited for the spatial scales required for water resource management. For regional groundwater monitoring, multispectral and microwave remotely sensed data together with land surface hydrological models are therefore required. Current global estimates of agricultural water use are still purely model based (Siebert and Döll 2010).

A detailed breakdown of anthropogenic water use in cities is not available globally, but case studies using an urban metabolism approach are available for a few cities (e.g., Sahely et al. 2003; Kenway et al. 2011). The best prospects for deriving urban-area specific data are from global modeling of integrated hydrological and water resources and demand at sufficient scale to resolve urban areas (e.g., Wada et al. 2014; Luck et al. 2015). Focus in these larger-scale models is on blue water use (water use related to irrigation, derived from groundwater, rivers, and lakes), but green (derived from natural precipitation and soil moisture) and gray water (water required to assimilate pollution) availability and use in cities is growing. New developments in urban climate modeling (Hamdi et al. 2020) and urban land surface characterization [World Urban Database and Access Portal Tools (WUADAPT); WUADAPT 2020] at meso- to microscale promise much better characterization of the urban water/energy balance, including some urban climate models that explicitly address the new developments in sustainable urban water supply (e.g., Broadbent et al. 2019).

Integrating water cycle components at various scales

The recent states and observed changes of Earth's water storage compartments are summarized in Table 1 and Fig. 1, while those of the annual fluxes are collected in Table 2 and Fig. 2. Even at these coarse scales, uncertainties of many of the components are large. Integrating a multiplicity of water cycle datasets into a single consistent dataset representative of the entire water cycle can help to optimize existing water cycle products or identify deficiencies in current observations.

Integration strategies. Dataset integration requires careful choices regarding the individual products of a single variable, the combination strategy, and appropriate spatial and temporal resolutions and domains. All these choices control if and how water cycle closure and consistency is eventually achieved. Ideally, coherence between water cycle products is already enforced at the retrieval stage (Popp et al. 2020; Lawford et al. 2004) but this is generally impractical given the many expert groups working on different water cycle components. Thus, their coherence is generally assessed a posteriori, either

- as a diagnostic of satellite product skill to quantify the sources of water imbalance and the uncertainties of each component (Sheffield et al. 2009; Moreira et al. 2019);
- to optimize the estimation of the components, using water budget closure as a constraint (Pan and Wood 2006; Munier et al. 2014); or
- to estimate missing information in the water cycle, e.g., an unobserved component (Azarderakhsh et al. 2011; Hirschi and Seneviratne 2017; Pellet et al. 2020) or an available component at a coarse resolution that requires downscaling (Ning et al. 2014).

The datasets can be combined in four ways:

- No optimization of the water components: Based on a priori knowledge on the quality of the data, single datasets of each water component are combined without modifying their values. This type of combination is used to study water cycle linkages or to diagnose the quality of the individual datasets (Sheffield et al. 2009; Moreira et al. 2019; Rodell et al. 2004).

Table 2. Summary of water cycle fluxes including trends. All values in $10^3 \text{ km}^3 \text{ yr}^{-1}$.

| Fluxes | ECVs involved | Yearly flux ($10^3 \text{ km}^3 \text{ yr}^{-1}$) | Uncertainty (1 sigma) | Uncertainty (%) | Reference | Global trends ($10^3 \text{ km}^3 \text{ yr}^{-2}$) | Trend uncertainty | Reference | Type of Observation |
|---|-------------------------|--|--|------------------|---|--|-------------------|---------------------------|------------------------------------|
| Precipitation over land | Precipitation | 1) 123.3, 2) 116.5 | 2) 5.4, 2) 5.1 | 1) 4.4%, 2) 4.4% | 1) Koutsoyiannis (2020), 2) Rodell et al. (2015) | Currently not detectable outside of noise | Not rated | Not rated | EO, in situ, reanalysis |
| Precipitation over ocean | Precipitation | 1) 399.4, 2) 403.5 | 1) 22.0, 2) 22.1 | 1) 5.5%, 2) 5.5% | 1) Koutsoyiannis (2020), 2) Rodell et al. (2015) | Currently not detectable outside of noise | Not rated | Not rated | EO, in situ, reanalysis |
| Land evaporation | Evaporation from land | 69.2 | 7.0 | 10% | Miralles et al. (2016) | 0.29 | 0.15 | Pan et al. (2020) | EO, in situ, reanalysis |
| Evaporation over ocean | Evaporation | 450.8 | 31.1 | 7% | Yu et al. (2017) | 0.66 | 0.20 | Yu et al. (2020) | EO, in situ, reanalysis |
| Atmospheric moisture transport from ocean to land | TCWV | 45.8 | 4.4 | 9.6% | Rodell et al. (2015), Schneider et al. (2017) | Not rated | Not rated | Not rated | Reanalysis |
| River discharge | River discharge | 1) 38.5, 2) 39.8 | 1.5 | ~4% | 1) Ghiggi et al. (2019) 2) Schmied et al. (2021) | Not rated | Not rated | Not rated | In situ + model |
| Groundwater discharge (fresh) | Groundwater | 0.5 | 0.3 | 60% | Y. Zhou et al. (2019) | Currently not detectable outside of noise | Not rated | Not rated | In situ + model |
| Groundwater recharge | Groundwater | 13.6 | 0.9 | ~13% | Mohan et al. (2018) | Not rated | Not rated | Not rated | Model, validated with in situ data |
| Glacier turnover 1) 1961–90, 2) 1980–2012 | Glacier | 1) 0.436, 2) 0.916 | 1) 0.273, 2) 0.273 | 1) 64%, 2) 32% | 1) Braithwaite and Hughes (2020), 2) Huss and Hock (2015); both studies estimate the flux from modeling; numbers are a combination of both flux and change in storage; density assuming 917 kg m^{-3} | Not rated | Not rated | Not rated | EO, in situ, reanalysis |
| Ice sheet turnover 1) West Antarctic, 2) East Antarctic, 3) Greenland ice sheet | Ice sheet | 1) + 2) -0.169, 3) -0.303 (2006–15), 1) + 2) -0.089, 3) -0.287 (2002–11) | 1) + 2) 0.021, 3) 0.012 (2006–15), 1) + 2) 0.029, 3) 0.023 (2002–11) | Not rated | IPCC (2019) | 1) + 2) -0.089 to -0.169, 3) -0.287 to -0.303 for 2002–11 to 2006–15 | Not rated | Not rated | EO, in situ |
| Permafrost water turnover | Permafrost | 4.3 | Not rated | Not rated | Shiklomanov et al. (2021) | +0.250 (1936–2015) | Not rated | Shiklomanov et al. (2021) | In situ, reanalysis |
| Groundwater extraction 1) flux-based method, 2) volume based | Anthropogenic water use | 1) 0.20, 2) 0.15 | 1) 0.03, 2) 0.04 | Not rated | Taylor et al. (2013) | Not rated | Not rated | Not rated | EO, in situ, reanalysis |
| Blue water irrigation | Anthropogenic water use | 2.7 | Not rated | Not rated | FAO (2021) | Not rated | Not rated | Not rated | National reporting |
| Domestic and industrial blue water use | Anthropogenic water use | 1.3 | Not rated | Not rated | Flörke et al. (2013) | +0.02 | Not rated | Flörke et al. (2013) | Modeling |

- Assimilation of the components into surface or hydrological models to ensure budget closure (Pan and Wood 2006; Pan et al. 2012; Sahoo et al. 2011; Zhang et al. 2018). This is a nontrivial task as it requires appropriate a priori bias correction, uncertainty estimates, and observation operators. Besides, it may impose model structures and dynamics on the observed variability.
- Statistical optimization between the components to force water budget closure without the use of a model (Rodell et al. 2015; Pellet et al. 2019; Aires 2014), which also requires estimates of dataset bias and uncertainties.
- Including energy budget constraints (Thomas et al. 2020; Rodell et al. 2015; Stephens et al. 2012).

Since not all water cycle components can be sufficiently well observed, their integration always requires data that are not purely observational, e.g., water vapor divergence from reanalysis or discharge estimates of ungauged basins estimated from an observation-driven hydrologic model (Pellet et al. 2019).

Water cycle integration across spatial and temporal scales. Water cycle integration can be done over a large range of spatial and temporal domains (appendix A, Table A3). The larger the scales, the lower the uncertainties of the individual inputs due to the averaging of errors, hence the easier it becomes to close the water budget. Rodell et al. (2015) made the first attempt to obtain globally consistent water and energy fluxes at a continental spatial resolution and for the climatological season, using satellite, in situ, and reanalysis data. The study highlighted the need for a snow measurement mission to better constrain the cold land hydrology as well as for a satellite mission dedicated to measuring evaporation to improve water budget closure over tropical areas. A water budget closure study performed over 341 basins around the world based on reanalysis and river discharge measurements raised the need of a mission dedicated to moisture convergence monitoring (Hirschi and Seneviratne 2017). Convergence estimates from reanalysis models are still better than any P estimates (Munier and Aires 2018; Rodell et al. 2011; Trenberth and Fasullo 2013; Trenberth et al. 2011), particularly over the tropics where E is too poorly observed or simulated by land surface models (Sahoo et al. 2011; Rodell et al. 2011; Munier and Aires 2018). Similar conclusions were recently reached by Koppa et al. (2021), based on a global assessment of P and E datasets in regards to their ability to simultaneously close energy and water budgets.

Regional water cycle integration studies have covered several parts of the world for various purposes but with mixed success. For South America, water budget integration has been used to estimate river discharge in several ungauged subbasins of the Amazon River (Azarderakhsh et al. 2011) and to assess continental closure (Moreira et al. 2019). In Africa, it was used to assess the water balance of the Volta basin (Ferreira and Asiah 2016) and Lake Victoria (Swenson and Wahr 2009). Mariotti et al. (2002) studied the long-term trends in water cycle components of the Mediterranean and estimated water flow through the Gibraltar Strait, which was later confirmed by a purely observation-based study (Pellet et al. 2019). Integrated water budget approaches were also used to quantify freshwater discharge from the entire pan-Arctic region (Syed et al. 2007; Landerer et al. 2010). For the United States it was shown that water budget closure from remote sensing only was not possible because of large errors in the individual products (Sheffield et al. 2009; Gao et al. 2012). Over Canada, a comprehensive climatology of the joint water and energy budgets was developed for the Mackenzie (Szeto et al. 2008) and Saskatchewan (Szeto 2007) River basins and later extended to the entire country (Wang et al. 2014, 2015). Liu et al. (2018) used water cycle integration to assess the seasonal cycles and trends (1982–2011) of the water budget components over the Tibetan Plateau while Pellet et al. (2020) reconstructed long-term (1980–2015) water storage

change over the main river basins in Southeast Asia and showed the dominant contribution of precipitation in its interannual variability.

At the pixel level, Zhang et al. (2018) created a 25-yr 0.5° resolution CDR at the global scale, using satellite observations, reanalysis data, and water cycle budget closure optimization. This CDR fits the need of a comprehensive database to describe the water cycle in a coherent way, but still at a coarse spatiotemporal resolution and heavily relying on hydrological modeling.

Example of global integration of state-of-the-art fluxes. Simple assessments at global and annual scales can be used to get a first grasp on the coherency between datasets. Here, we use a description of the terrestrial water cycle budget integrated over all continental surfaces, i.e., the change in TWS ($dTWS$) = terrestrial precipitation (Pt) – terrestrial evaporation (Et) – discharge (R); R includes both river (Rr) and groundwater discharge (Rg), which is difficult to estimate directly. But, when assuming that $dTWS$ equals zero at the annual scale, Rg can be estimated from the state-of-the-art numbers reported in this study by

$$R_g = dTWS + Pt - Et - R_r = 0 + 123,300 - 69,200 - 39,981 = 14,119 \pm 9,004 \text{ } 10^3 \text{ km}^3 \text{ yr}^{-1}.$$

The uncertainty estimate is derived by standard error propagation of uncorrelated Gaussian-distributed errors. Despite the very large uncertainty range, it does not cover the state-of-the-art Rg estimate ($0.5 \pm 0.3 \text{ } 10^3 \text{ km}^3 \text{ yr}^{-1}$; Table 2). Biases in the individual components directly translate into a biased discharge estimate, while it is difficult to attribute this imbalance to a specific dataset. Also, uncertainties in each product are crucial to weigh certain datasets over uncertain ones, and to estimate a posteriori the uncertainty of the final solution. While combining yearly data at the global scale reduces uncertainties thanks to the canceling of errors, and the above representation may be too simplistic, e.g., assuming $dTWS = 0$, it does show that we are still far from perfect closure based on observations only, even at these coarse scales. This becomes increasingly challenging at finer spatial and temporal scales.

The water budget cannot be accurately closed if one of the components is not observed. This is even more so the case for the long-term trends (Tables 1 and 2). Global trend estimates are still too uncertain for many components, because of too short observation records or failing intercalibration of sensors over time. Besides, closing trends in the water cycle components requires a sufficiently long common baseline period, which is currently lacking for the ECVs that do provide trends based on scientific consensus (Tables 1 and 2). Yet various studies assessed trends and their underlying drivers in multiple observations of individual ECVs, often in combination with trends in reanalysis products, e.g., for precipitation (Zhang et al. 2007), soil moisture (Preimesberger et al. 2020), land evaporation (Y. Zhang et al. 2016), and runoff (Yang et al. 2019). Several recent studies demonstrated consistency in trends between a selection of water cycle ECVs, mostly between continental ice melt and sea level rise (Zemp et al. 2019; Shepherd et al. 2020; Raj et al. 2020), but substantial uncertainty remains for the land water storage components (Cazenave et al. 2018).

Synthesis and outlook

Long-term monitoring Earth's water cycle has made great progress in recent decades, but many observational gaps still need to be overcome to fully characterize variability in individual components and allow for a comprehensive and consistent assessment of the water cycle as a whole. Tables 3 and 4 summarize the main challenges per water cycle component [status and long-term changes (trends) of both, the changes in storage but also changes in fluxes as available] confronted with the foreseen observational and methodological developments. Several challenges shared by multiple water cycle components are summarized in the following.

Table 3. Summary capability demands and outlook of water cycle storages.

| Storage | Observational needs | | Observational outlook | | Other (methodological developments, reanalysis, etc.) |
|---|---|---|--|--|--|
| | In situ | EO | In situ | EO | |
| Oceans | Enhance the Argo array of profiling floats including full-depth Argo to estimate the contribution of deep-ocean warming and salinity changes | Ensure the continuity of satellite altimetry beyond 2030; ensure the continuity of satellite gravimetry and surface salinity missions | Establishment of a fully global, top-to-bottom, dynamically complete, and multidisciplinary Argo program | Constellation of satellite altimetry for sea level and satellite radiometry for sea surface salinity; the CIMR mission concept can provide continuity for satellite salinity measurements | A suite of ocean reanalysis products that assimilate various in situ and EO measurements for ocean ECVs; in the future Argo will integrate seamlessly with satellite and with other in situ elements |
| Terrestrial open water (lakes, artificial reservoirs, wetlands) | Determine the exact quantity of water from lakes and wetlands that contribute to global closure of the water cycle; more precise and more frequent updates of hypsometry curves needed | Ensure the continuity of high-resolution satellite altimetry beyond 2030 | | SWOT mission for characterization or water table depth of smaller lakes; Sentinel-1 and Sentinel-2 satellites will greatly complement existing series of Landsat images used for hypsometry curves | Focus on a set of representative lakes that most objectively reflect the climatic signal |
| Atmospheric water vapor | More in situ measurements are needed over oceans and in the Southern Hemisphere | Improved satellite-based measurements to measure water vapor over land during cloudy conditions, in the lower troposphere and the boundary layer; dedicated mission for moisture convergence monitoring | Increased number of frost point hygrometer launch sites as part of the GRUAN network | CrIS and ATMS instruments for JPSS-3 and JPSS-4; IASI-NG, METImage, MWI, and MWS on EPS-SG, AMSR-3 on GOSAT-GW | Reanalysis models must be improved to maintain water mass balance |
| Groundwater | Maintain and extend in situ national groundwater level monitoring networks to close observational gaps (particularly in the Global South) and promote data sharing among countries | Higher spatial resolution to monitor smaller aquifers; long-term observing system | Establishment of new national groundwater monitoring programs | Next-generation global gravity satellite missions with increased spatial resolution planned | Improved modeling and downscaling of groundwater variations using machine learning |
| Soil moisture | Expand capabilities to under-represented regions (e.g., Africa, southern America) and climates that are currently poorly covered (e.g., monsoon, tropic, polar); clever, dense network design to bridge scale gaps | Continuation of dedicated L-band soil moisture missions; improved spatial resolution | Establishment of fiducial reference networks (ESA, Copernicus) | CIMR L band, Tandem-L, ROSE-L, HydroTerra for diurnal variability, high-resolution products from downscaling and SAR satellites | Better retrievals and models for dense vegetation and organic soils |
| Glaciers | Additional multitemporal glacier inventories every ~20 years; better spatial coverage of glacier thickness measurements; at least one long-term mass-balance monitoring program in every larger mountain range providing glaciological variability at seasonal to annual time resolution | Close geodetic gaps in regions where glaciers dominate runoff during warm/dry seasons, e.g., in the tropical Andes and in Central Asia, and in the heavily glacierized regions dominating the glacier contribution to sea level rise, i.e., Alaska, Arctic Canada, Russian Arctic, Greenland and Antarctica | Maintain and expand worldwide in-situ network with a focus on long-term monitoring programs. | Spaceborne altimetry (<i>ICESat-2</i>); increasing availability of large-scale high-resolution DEMs; unlock national archives of aerial surveys and photogrammetric processing of early optical satellite data | Exploit reconstructions from topographic maps and geomorphological evidence |
| Ice sheets and ice shelves | International coordinated observation flight campaigns to cover the “missing areas” along major outlet glaciers, particularly in East Antarctica; Surface traverse campaigns for improving firn models and englacial hydrology, especially in Greenland with its increasing seasonal melt zones | Continuation and effective combination of various existing satellite programs, e.g., <i>ICESat-2</i> , <i>CryoSat</i> , and future ESA Crystal missions | Campaigns in Greenland and Antarctica for satellite validation; need to close observational gap with unknown outlet glacier thickness in East Antarctica | ESA Crystal mission, Copernicus CMIR, Copernicus Polar Ice and Snow Topography Altimeter (CRISTAL), and ROSE-L | Need of more diverse atmosphere reanalysis products, e.g., snow densities, firn compactions, snow drift and surface conditions, to narrow down ice sheet mass change models |

Table 3. Continued.

| Storage | Observational needs | | Observational outlook | | Other (methodological developments, reanalysis, etc.) |
|------------|--|--|--|--|--|
| | In situ | EO | In situ | EO | |
| Permafrost | The main difficulty for assessing permafrost distribution, ice content and mass changes is that permafrost is not visible at the surface | Still no reliable remote sensing technique for detecting permafrost; need for a surface subsidence product | Spatial observational gaps have to be filled | Tentatives are in progress within the ESA/CCI project | Most urgent need is a sustainable and reliable funding of monitoring networks and the database infrastructure, ensuring long-term availability of observational data |
| Snow | Expand ground-based observation networks | Continuation of satellite programs | | CIMR is expected to provide SWE at improved accuracy and resolution; SAR based approaches (e.g., Sentinel-1) for mapping snow mass and SWE in mountain areas | Fusing observations from active and passive sensors or combining them with independent reference data |

Table 4. Summary capability demands and outlook of water cycle fluxes.

| Flux | Observational needs | | Observational outlook | | Other methodological developments, reanalysis, etc. |
|---------------------|--|---|---|---|---|
| | In situ | EO | In situ | EO | |
| Ocean evaporation | Near-surface observations with focus on air temperature and humidity | Improved satellite retrieval algorithms for near-surface ECVs with focus on air temperature and humidity | Explore the use of air-sea observations from new autonomous platforms such as saildrones and wave gliders; sustained and expand existing surface buoy network | Continuity of microwave imager programs via, e.g., EUMETSAT (EPS-SG) and JAXA (GOSAT-GW) and NOAA JPSS (ATMS) | Improvement of the model constraint of the ocean $E-P$ estimates and the model-data synthesis capability of EO to the ocean water cycle; reconcile large spread in atmospheric reanalysis models and satellite gridded products |
| Land evaporation | Novel means to measure interception loss over multiple ecosystems | Missions dedicated to measuring evaporation to improve water budget closure over tropical, semiarid and high-latitude areas | Use of data from new in situ networks such as SAPFLUXNET (http://sapfluxnet.creaf.cat) in combination with eddy-covariance data | New types of EO (such as solar induced chlorophyll fluorescence) and new platforms (such as CubeSats and UAVs) | |
| Ocean precipitation | | Retrieval skills need to be improved, to address intermittent nature and high spatial and temporal variability of precipitation | | Continuity of microwave imager and sounder programs via, e.g., EUMETSAT (EPS-SG), JAXA (GOSAT-GW) and NOAA (JPSS); NASA-JAXA PMM; improved snow retrieval capabilities with ICI (EUMETSAT, EPS-SG), largely improved temporal sampling with the TROPICS mission (NASA); new microwave imager mission CIMR (ESA) | Integration of multiple sensors and deriving reanalysis products will address the high spatial and temporal variability |
| Land precipitation | Improve timeliness to contribute precipitation data to GPCP | Improved consistent long-term datasets | | Same as for ocean precipitation | Integration of multiple sensors (in situ, remote sensing) and techniques (rain gauges, meteorological radars, soil moisture) |
| River discharge | Improve timeliness to contribute data to GTN-R; long-term, regular measurements of upstream river discharge on finer spatial scale | Increase numbers of virtual stations from altimetry | In situ observations are globally under threat due to reduced field observation capabilities and priorities | SWOT for measuring rivers wider than 100 m; SWOT assimilation into models to derive first globally consistent information on river discharge | Data integration and assimilation methods will be used to provide information on river discharge based on different sensors and observation techniques |

Table 4. Continued.

| Flux | Observational needs | | Observational outlook | | Other methodological developments, reanalysis, etc. |
|--|---|--|---|--|---|
| | In situ | EO | In situ | EO | |
| Groundwater discharge from continents to ocean | Increase number and frequency of observations of groundwater discharge | Better understanding of usefulness of EO for groundwater discharge monitoring | Advances in geophysical tools, which can be coupled with hydrological flow modeling | | Model simulations are becoming more skillful due to increasing availability of high-quality hydrologic and topographic data that feed them |
| Glacier and ice sheet turnover | To understand rapid changes in ice mass flux and ice instability the observation of bottom melting is essential | | Close coordination as diverse as Earth rheology and geophysics (for heat flow modeling), glaciology for understanding ice movements, crevassing and calving, meteorology for snowfall and firn compaction is required | Broadband observation from visual to L-band radar active measurements, and passive microwave observations sensitive to surface melting | Improved estimations of glacier mass turnover require a better integration of observations into numerical models with full representation of individual glaciers |
| Anthropogenic water use | Irrigation surveys available at subnational scale, with shorter delivery time | Improved spatial and temporal resolution of microwave observations for soil moisture retrieval | | The revisit time will improve after launch of two new Sentinels, i.e., Sentinel-1C and Sentinel-1D, planned for 2022 and 2023; ESA Earth Explorer HydroTerra for subdaily observations | Downscaling of coarse satellite soil moisture to resolve elements of anthropogenic water use; integrated modeling approaches for resolving anthropogenic water use at the necessary scale and temporal resolution, with accounting and satellite data used for input and validation |

Continuation and expansion of existing observation systems. If at all, trends in water cycle components can only be observed with great uncertainty, which is mainly due to insufficient length and homogeneity of the observations. Thus, it is of utmost performance to restore historical satellite and ground data, continue existing measurement concepts and harmonize past, current and future observing systems. Even satellite observing systems with demonstrated skill for a range of variables (e.g., L-band radiometer observations for soil moisture and vegetation water, gravity observations for groundwater, ice sheets, and glaciers) have an uncertain future. The joint CEOS/CGMS working group Climate supports a strategic planning beyond the lifetime of a single mission. The EUMETSAT's Satellite Application Facilities and the joint EC/ESA-Copernicus programs are already in line with this paradigm shift.

A major difficulty is the intercalibration of satellite datasets with varying quality and temporal/spatial characteristics over time. Yet as shown by this review, satellites alone cannot solve for the entire balance and coordinated ground monitoring capacities are needed. Extensive networks of long-term fiducial in situ monitoring networks are fundamental in this respect, e.g., those federated within the Global Terrestrial Network for Hydrology (GTN-H; <https://www.gtn-h.info/>), the Global Ocean Observing System (GOOS; <https://www.goosocean.org/>), and the Global Atmosphere Watch (GAW; <https://public.wmo.int/en/programmes/global-atmosphere-watch-programme>). However, their ambition to collect trustworthy observations worldwide is encumbered by lacking open data policies and the fact that many ground observing networks heavily rely on scientific project funding, causing observational gaps particularly in the global south. Support and advocacy for the national hydrological and meteorological services as well as space agencies to fund, collect, and make available these data must be expanded.

New observation systems. Several dedicated scientific satellite missions have been scheduled to fill existing gaps in water cycle observations, among them SWOT (Morrow et al. 2019), scheduled for launch in 2021. SWOT is expected to revolutionize continental water cycle observability, by allowing the global characterization of lake and river discharge dynamics in regions with sparse ground monitoring or restrictive data sharing policies. Apart from the Sentinel satellites currently in orbit or already scheduled for launch, the EU-Copernicus program has defined several High Priority Candidate missions, of which CIMR, CRISTAL, and ROSE-L have particular relevance for improved characterization of various water cycle components, including snow, ice sheets and shelves, glaciers, and soil moisture. In addition, new EO observation capabilities need to be developed for ECVs that thus far are hardly characterized, e.g., ground ice, anthropogenic water use, and groundwater recharge and discharge. Yet by nature, these components will heavily rely on ground observations and consequently adequate ground infrastructure needs to be established, improved, and sustainably supported. In addition, artificial intelligence and machine learning should become routinely applied for reduction of retrieval errors and uncertainties of upcoming and existing missions.

Integration of ECVs with other components and models. In general, the integration of existing sensors (in situ, remote sensing) and techniques will close observational gaps. A new ECV total terrestrial water storage (TWS) would provide more timely and integrative data to directly close the continental water budget of P , E , R , and $dTWS$ (see “Integrating water cycle components at various scales” section). A long-term perspective for gravity observations from space is thus crucial.

But no matter how sophisticated the satellites or observing systems are, observation errors in the individual products will always be present and lead to inconsistencies between ECVs, hampering a comprehensive assessment of the water cycle. Statistical integration methods can force consistency between ECVs and optimize individual components, but require estimates of their uncertainties, which are not trivial to obtain. Also data integration methods can profit from artificial intelligence and machine learning to reduce uncertainties and biases (Aires 2018). For instance, Beck et al. (2021) used ancillary data of surface properties in a random forest machine learning framework to explain errors at the pixel level while closing the water budget. Such an approach can be trained at basins where sufficient (most importantly discharge) data are available to close the water budget and then applied to each location or pixel for which this requirement is not fulfilled. Structural errors (biases) can be state dependent (e.g., for anthropogenic water use or discharge), have spatial or seasonal patterns, and directly translate into an imbalance in the water budget. Higher spatial and temporal resolutions may reveal important local climate signals, e.g., on extreme events, but closing the water budget at these scales becomes increasingly challenging. State-of-the-art closure methods analyze regions at the subbasin scale, requiring knowledge of the interdependency of the subbasins and the lateral (sub-)surface transport (Azarderakhsh et al. 2011; Pellet et al. 2020). This interdependency of subbasins can be pushed even further to the pixel scale, but the spatial resolution of some datasets (e.g., GRACE) is a major limitation. However, integrating the datasets and imposing the budget closure can actually be a technical solution to downscale coarse resolution datasets, both spatially and temporally (Ning et al. 2014).

Improving model–data synthesis capabilities and reducing the spread of reanalysis products on precipitation, evaporation, and discharge is needed for an advanced closure of the water cycle, in particular at regional to local scales. This can be achieved by consolidating forcing data and auxiliary datasets, e.g., by using a common land–sea mask (Popp et al. 2020) or by constraining reanalyses with observations, e.g., satellite-observed ocean salinity (Yu et al. 2017).

This especially applies to the uncertainty of atmospheric moisture transport, which cannot be measured directly and is mostly inferred from reanalysis. Different approaches to model key elements (e.g., terrestrial interception loss) explain for some ECVs the lack of global closure in the water cycle. It is also concluded that integrated modeling approaches provide the best prospect for resolving anthropogenic water use at the necessary scale and temporal resolution, with accounting and satellite data used for input and validation.

Final remarks. Available and clean water resources are one of our biggest challenges globally and are under pressure due to global change (UNESCO 2020). This requires consistent monitoring and long-term observation strategies. Water is a connecting element, but it is also the focus of various competing interests that can lead to serious political conflicts. While observational needs are currently expressed by the individual communities, the definition of future observation systems should consider following a more holistic approach and observe water cycle components as part of their global cycle and assess its variability in conjunction with the energy and carbon cycles. This should be adopted and implemented by high level organizations like GCOS, but also by the agendas of the WMO member states as well as of the WMO research agenda.

Acknowledgments. WD acknowledges ESA's QA4EO (ISMN) and CCI Soil Moisture projects. WD, CRV, AG, and KL acknowledge the G3P project, which has received funding from the European Union's Horizon 2020 research and innovation programme under Grant Agreement 870353. MIH and MS acknowledge ESA's CCI Water Vapour project. MS and RH acknowledges the support by the EUMETSAT member states through CM SAF. DGM acknowledges support from the European Research Council (ERC) under Grant Agreement 715254 (DRY-2-DRY).

Part of this research was carried out at the Jet Propulsion Laboratory, California Institute of Technology, under a contract with the National Aeronautics and Space Administration (80NM0018D0004).

We thank Gabi Hegerl and Robert Reinecke for their advice on the manuscript and Andrea Wessler for graphic editing. We thank Thomas Frederikse for providing the trends and uncertainties of water stored in oceans based on the results of Frederikse et al. (2020). We also would like to thank Marianne Nail (<https://girlsmakesense.com/>) for allowing us to use her figures as basis for the development of Figs. 1 and 2. Finally, we thank the three anonymous reviewers for their very valuable suggestions for improvement and Peter Blanken for his editing.

Data availability statement. No data are used in this study.

Appendix A: Summary of (semi-)operational long-term global observing systems and large-scale water cycle studies

Supporting information for this study is organized as follows:

- Table A1 presents a summary of (semi-)operational long-term global observing systems and programs of water cycle storages.
- Table A2 presents a summary of (semi-)operational long-term global observation systems and programs of water cycle fluxes.
- Table A3 presents a summary of observation-based large-scale water cycle studies.

Table A1. Summary of (semi-)operational long-term global observing systems and programs of water cycle storages.

| Storage | GCOS ECVs involved | In situ | EO |
|----------------------------|---|---|--|
| Oceans | Sea level, sea surface and subsurface temperature (suggested as possible future ECV: ocean mass, ocean bottom pressure) | Global Sea Level Observing System (GLOSS) (gloss-sealevel.org/data/) International Comprehensive Ocean–Atmosphere Dataset (ICOADS) (rda.ucar.edu/datasets/ds548.0/); UKMO EN4 subsurface temperature and salinity (metoffice.gov.uk/hadobs/en4/) | JPL PO.DAAC: (podaac.jpl.nasa.gov/OceanSurfaceTopography); ESA CCI sea level (climate.esa.int/odp); ESA CCI sea surface temperature (climate.esa.int/odp); Copernicus Marine Service (marine.copernicus.eu); Group for High Resolution Sea Surface Temperature (ghrsst.org); |
| Lakes and reservoirs | Lakes | International Data Centre on Hydrology of Lakes and Reservoirs (hydrolare.net/) hosts the GTN-L as part of GTN-H | Hydroweb (legos.obs-mip.fr/soa/hydrologie/hydroweb/) as part of GTN-H ESA CCI Lakes (climate.esa.int/odp) Copernicus Global Land Surface (land.copernicus.eu/) |
| Atmospheric water vapor | Water vapor | Hadley Centre Integrated Surface Database (HadISD) (metoffice.gov.uk/hadobs/hadisd/); ICOADS (rda.ucar.edu/datasets/ds548.0/); Integrated Surface Database (ISD) of the NCEI of NOAA (ncdc.noaa.gov/isd/data-access) | Copernicus Atmosphere Monitoring Service (atmosphere.copernicus.eu/) EUMETSAT CM SAF (cmsaf.eu) ESA CCI Water Vapor (climate.esa.int/odp) Remote Sensing Systems (remss.com) |
| Groundwater | Groundwater | Global Groundwater Monitoring Network (un-igrac.org/special-project/ggmn-global-groundwater-monitoring-network) hosted by IGRAC and part of GTN-H | none; Global Gravity-based Groundwater Product G3P (www.g3p.eu) in preparation |
| Soil moisture | Soil moisture | International Soil Moisture network and part of GTN-H (ismn.geo.tuwien.ac.at/ ; ismn.Earth) | ESA CCI Soil Moisture (climate.esa.int/odp); C3S soil moisture (cds.climate.copernicus.eu/) |
| Permafrost | Permafrost | Global Terrestrial Network–Permafrost (GTN-P) | None |
| Glaciers | Glaciers | U.S. National Snow and Ice Data Center (nsidc.org) as part of GTN-G (gtn-g.org); World Glacier Monitoring Service (wgms.ch) as part of GTN-G (https://www.gtn-g.org) | U.S. National Snow and Ice Data Center; World Glacier Monitoring Service as part of GTN-G; ESA CCI Glaciers (climate.esa.int/odp) |
| Ice sheets and ice shelves | Ice sheets and ice shelves | National Snow and Ice Data Center PROMICE (promice.dk) | Satellite ECV Inventory by the CEOS/CGMS Working Group on Climate (WGClimate) (climatemonitoring.info/ecvinventory); ESA CCI Greenland and Antarctica ice sheets (climate.esa.int/odp); C3S ice sheets (cds.climate.copernicus.eu/) |
| Snow | Snow | National Snow and Ice Data Center; Global Snow Laboratory (climate.rutgers.edu/snowcover/) | ESA CCI Snow (climate.esa.int/odp) Copernicus Global Land Service (land.copernicus.eu) |
| Living biomass | Above-ground biomass | None | ESA Globbiomass (globbiomass.org/); ESA CCI Biomass project (climate.esa.int/odp); NASA Carbon Monitoring Systems (carbon.nasa.gov/) |

Table A2. Summary of (semi-)operational long-term global observation systems and programs of water cycle fluxes.

| Flux | GCOS ECVs involved | In situ | EO |
|--------------------------------|--|--|--|
| Ocean evaporation | Sea surface temperature; wind speed; air temperature; air humidity | GLOSS (gloss-sealevel.org/data/); ICOADS (rda.ucar.edu/datasets/ds548.0/) | JPL PO.DAAC (podaac.jpl.nasa.gov/OceanSurfaceTopography) CM SAF (10.5676/EUM_SAF_CM/HOAPS/V002) ESA CCI Sea Level (climate.esa.int/odp); ESA CCI Sea Surface Temperature (climate.esa.int/odp); SEAFLEX (http://seaflex.org) Cross-calibrated multiplatform (CCMP) gridded surface vector winds (www.remss.com) Copernicus Marine Service (marine.copernicus.eu/) |
| Land evaporation | Evaporation from Land | FLUXNET (fluxnet.ornl.gov) SAPFLUXNET (http://sapfluxnet.creaf.cat) | MOD16 (ladsweb.modaps.eosdis.nasa.gov/search/order/2/MOD16A2-6); Global Land Evaporation Amsterdam Model (GLEAM; gleam.eu); |
| Ocean precipitation | Precipitation | OceanRAIN (oceanrain.cen.uni-hamburg.de/) | GPCP (psl.noaa.gov); PERSIANN (https://data.nodc.noaa.gov/); IMERG (gpm.nasa.gov/) CM SAF (HOAPS CDRs; 10.5676/EUM_SAF_CM/HOAPS/V002) IPWG at www.isac.cnr.it/~ipwg/data/datasets.html . |
| Land precipitation | Precipitation | GPCC (opendata.dwd.de/climate_environment/GPCC/html/download_gate.html); ISD of NCEI NOAA (ncdc.noaa.gov/isd/data-access); Global Historical Climatology Network (GHCN) of NCEI NOAA (ncdc.noaa.gov/data-access/land-based-station-data/land-base) | As for ocean precipitation |
| River discharge | River discharge | WMO Hydrological Observing System (wmo.int/pages/prog/hwrrp/chy/whos/index.php) Global Runoff Data Base (GRDC) (portal.grdc.bafg.de/); the Global River Discharge (RivDIS) Project (rivdis.sr.unh.edu) | None |
| Groundwater discharge | Groundwater | None | None |
| Glacier and ice sheet turnover | Glaciers; ice sheets and ice shelves | None | None |
| Anthropogenic use | | FAO AQUASTAT (fao.org/aquastat/en/databases/) as part of GTN-H | None |

Table A3. Summary of observation-based large-scale water cycle studies. EO means that multiple satellite observations are used for the same water component to quantify the uncertainty in these.

| Reference | Temporal resolution | Spatial resolution | Spatial domain | Temporal domain | Objective | Input data | Combination method |
|--------------------------------|---------------------|------------------------------------|----------------|-----------------|---|--------------------------------|---|
| Rodell et al. (2004) | Monthly | 1 basin Mississippi | Regional | 14 months | Estimate ET from GRACE | EO, in situ, reanalysis | No optimization land |
| Rodell et al. (2011) | Monthly | 7 basins | Global | 8 years | Estimate ET uncertainty | EO, in Situ, reanalysis | No optimization land |
| Azarderakhsh et al. (2011) | Monthly | Multiple subbasins over the Amazon | Regional | 4 years | Estimate river discharge and spatial analysis | EO, in situ | No optimization land |
| Hirschi and Seneviratne (2017) | Monthly | 341 basins | Global | 20 years | Long-term estimation of change in storage | In situ, reanalysis | No optimization land+atmosphere |
| Mariotti et al. (2002) | Climatology | Basin and pixel over Mediterranean | Regional | 20 years | Estimation Gibraltar Strait netflow | EO, in situ, reanalysis | No optimization ocean+atmosphere |
| Sheffield et al. (2009) | Monthly | 1 basin Mississippi | Regional | 2 years | Water budget imbalance | EO, in situ | No optimization land |
| Moreira et al. (2019) | Monthly | Basin and pixel over South America | Continental | 10 years | Water budget imbalance | EO, in situ | No optimization land |
| Rodell et al. (2015) | Climatologic season | Continental | Global | 10 years | Optimize global fluxes | EO, in situ, reanalysis, model | Optimal interpolation land+atm.+ocean with energy cycle |
| Pan et al. (2012) | Monthly | 32 basins | Global | 20 years | Optimize long-term fluxes | EO, in situ, reanalysis, model | Assimilation land |
| Pellet et al. (2019) | Monthly | Subbasins over Mediterranean | Regional | 8 years | Optimize regional water cycle | EO, in situ, reanalysis | Optimal interpolation land+atm.+ocean |
| Munier and Aires (2018) | Monthly | 9 basins | Global | 8 years | Optimize and error analysis | EO, in situ | Optimal interpolation land |
| Sahoo et al. (2011) | Monthly | 10 basins | Global | 3 years | Optimize using satellite only data | EO, in situ, model | Assimilation land |
| Shiklomanov et al. (2021) | Seasonal | Basins | Pan-Arctic | 30–50 years | Estimate change in river discharge | In situ | |
| Zhang et al. (2018) | Monthly | 0.5° pixel | Global | 25 years | Climate Data Record | EO, model | Y. Zhang et al. (2016) |

Appendix B: Acronyms used in this study

| | |
|---------------|---|
| Aeolus | ESA Satellite mission |
| AGB | Above-ground biomass |
| AMRS-2 | Advanced Microwave Scanning Radiometer 2 |
| ASCAT | Advanced Scatterometer |
| AVHRR | Advanced Very High Resolution Radiometer |
| BGB | Below-ground biomass |
| C3S | Copernicus Climate Change Service |
| CDR | Climate Data Record |
| CGD | Coastal groundwater discharge |
| CIMR | Copernicus Imaging Microwave Radiometer |
| CRISTAL | Copernicus Polar Ice and Snow Topography Altimeter |
| <i>dS</i> | Total terrestrial storage change |
| <i>E</i> | Evaporation |
| ECV | Essential climate variable |
| EOS | Earth Observing System |
| ESA | European Space Agency |
| ESA CCI | ESA Climate Change Initiative |
| CryoVEx | CryoSat2 Validation Experiment |
| ET | Evapotranspiration |
| Et | Terrestrial evaporation |
| EUMETSAT | European Organisation for the Exploitation of Meteorological Satellites |
| FAO | Food and Agriculture Organization |
| FTIR | Fourier-transform-infrarot-spektrometer |
| GAW | Global Atmosphere Watch |
| GCOS | Global Climate Observing System |
| GDL | Groundwater discharge to lakes |
| GEO | Geostationary orbit |
| GGMN | Global Groundwater Monitoring Network |
| GMSL | Global mean sea level |
| GOOS | Global Ocean Observing System |
| GPPC | Global Precipitation Climatology Centre |
| GPM | Global Precipitation Measurement Satellite |
| GPS | Global positioning system |
| GRACE | Gravity Recovery and Climate Experiment |
| GRACE-FO | GRACE Follow-On |
| GRDC | Global Runoff Data Centre |
| GRUN | Global gridded runoff data |
| GTN-G | Global Terrestrial Network for Glaciers |
| GTN-H | Global Terrestrial Network for Hydrology |
| GTN-P | Global Terrestrial Network for Permafrost |
| GTN-R | Global Terrestrial Network for Rivers |
| <i>ICESat</i> | <i>Ice, Cloud and land Elevation Satellite</i> |
| ICWRGC | International Centre for Water Resources and Global Change |
| InSAR | Interferometry of Synthetic Aperture Radar |
| IPCC | Intergovernmental Panel on Climate Change |
| JAXA | Japan Aerospace Exploration Agency |
| LEO | Low-Earth orbit |
| Lidar | Light detection and ranging |
| MERRA-2 | Modern-Era Retrospective Analysis for Research and Applications |

| | |
|------------|--|
| MetOp | Meteorological Operational Satellite |
| MRMS | Multi-Radar Multi-Sensor |
| NGD | Nearshore terrestrial groundwater discharge |
| JPSS | Joint Polar Satellite System |
| NSIDC | National Snow and Ice Data Center |
| <i>P</i> | Precipitation |
| Pt | Terrestrial precipitation |
| <i>R</i> | All discharge |
| RACMO | Regional Atmospheric Climate Model |
| Rg | Groundwater discharge |
| RH | Relative humidity |
| root:shoot | Ratio of below- and above-ground biomass |
| ROSE-L | L-band Synthetic Aperture Radar |
| Rr | River discharge |
| SAR | Synthetic Aperture Radar |
| SGD | Submarine groundwater discharge |
| SMAP | Soil Moisture Active Passive |
| SMMR | Scanning Multichannel Microwave Radiometer |
| SMOS | Soil Moisture Ocean Salinity |
| SROCC | Special Report on the Ocean and Cryosphere in a Changing Climate |
| SSM/I | Special Sensor Microwave Imager |
| SST | Sea surface temperature |
| SWE | Snow water equivalent |
| SWOT | Surface Water Ocean Topography |
| TCWV | Total column water vapor |
| TIRS | Thermal infrared sensors |
| TPW | Total precipitable water |
| TRMM | Tropical Rainfall Measuring Mission |
| TWS | Total terrestrial water storage |
| UN | United Nations |
| UNFCCC | United Nations Framework Convention on Climate Change |
| VOD | Vegetation optical depth |

References

- Abbott, B. W., and Coauthors, 2019: Human domination of the global water cycle absent from depictions and perceptions. *Nat. Geosci.*, **12**, 533–540, <https://doi.org/10.1038/s41561-019-0374-y>.
- Abolafia-Rosenzweig, R., M. Pan, J. L. Zeng, and B. Livneh, 2021: Remotely sensed ensembles of the terrestrial water budget over major global river basins: An assessment of three closure techniques. *Remote Sens. Environ.*, **252**, 112191, <https://doi.org/10.1016/j.rse.2020.112191>.
- Aires, F., 2014: Combining datasets of satellite-retrieved products. Part I: Methodology and water budget closure. *J. Hydrometeor.*, **15**, 1677–1691, <https://doi.org/10.1175/JHM-D-13-0148.1>.
- , 2018: Atmospheric water vapour profiling over ocean/land and for clear/cloudy situations using microwave observations. *Remote Sensing of Clouds and Precipitation*, Springer, 215–255.
- Albergel, C., and Coauthors, 2013: Skill and global trend analysis of soil moisture from reanalyses and microwave remote sensing. *J. Hydrometeor.*, **14**, 1259–1277, <https://doi.org/10.1175/JHM-D-12-0161.1>.
- Alexander, L. V., M. Bador, R. Roca, S. Contractor, M. G. Donat, and P. L. Nguyen, 2020: Intercomparison of annual precipitation indices and extremes over global land areas from in situ, space-based and reanalysis products. *Environ. Res. Lett.*, **15**, 055002, <https://doi.org/10.1088/1748-9326/ab79e2>.
- Allan, R. P., and Coauthors, 2020: Advances in understanding large-scale responses of the water cycle to climate change. *Ann. N. Y. Acad. Sci.*, **1472**, 49–75, <https://doi.org/10.1111/nyas.14337>.
- Asner, G. P., and Coauthors, 2012: High-resolution mapping of forest carbon stocks in the Colombian Amazon. *Biogeosciences*, **9**, 2683–2696, <https://doi.org/10.5194/bg-9-2683-2012>.
- Avitabile, V., and Coauthors, 2016: An integrated pan-tropical biomass map using multiple reference datasets. *Global Change Biol.*, **22**, 1406–1420, <https://doi.org/10.1111/gcb.13139>.
- Azarderakhsh, M., W. B. Rossow, F. Papa, H. Norouzi, and R. Khanbilvardi, 2011: Diagnosing water variations within the Amazon basin using satellite data. *J. Geophys. Res.*, **116**, D24107, <https://doi.org/10.1029/2011JD015997>.
- Babaeian, E., M. Sadeghi, S. B. Jones, C. Montzka, H. Vereecken, and M. Tuller, 2019: Ground, proximal, and satellite remote sensing of soil moisture. *Rev. Geophys.*, **57**, 530–616, <https://doi.org/10.1029/2018RG000618>.
- Bamber, J. L., and A. Rivera, 2007: A review of remote sensing methods for glacier mass balance determination. *Global Planet. Change*, **59**, 138–148, <https://doi.org/10.1016/j.gloplacha.2006.11.031>.
- , R. M. Westaway, B. Marzeion, and B. Wouters, 2018: The land ice contribution to sea level during the satellite era. *Environ. Res. Lett.*, **13**, 063008, <https://doi.org/10.1088/1748-9326/aac2f0>.
- Baumgartner, A., and E. Reichel, 1975: *Die Weltwasserbilanz: Niederschlag, Verdunstung und Abfluß über Land und Meer sowie auf der Erde im Jahresdurchschnitt*. R. Oldenbourg Verlag, 197 pp.
- Beck, H. E., and Coauthors, 2021: Evaluation of 18 satellite- and model-based soil moisture products using in situ measurements from 826 sensors. *Hydrol. Earth Syst. Sci.*, **25**, 17–40, <https://doi.org/10.5194/hess-25-17-2021>.
- Berg, A., and J. Sheffield, 2019: Evapotranspiration partitioning in CMIP5 models: Uncertainties and future projections. *J. Climate*, **32**, 2653–2671, <https://doi.org/10.1175/JCLI-D-18-0583.1>.
- Berghuijs, W. R., R. A. Woods, and M. Hrachowitz, 2014: A precipitation shift from snow towards rain leads to a decrease in streamflow. *Nat. Climate Change*, **4**, 583–586, <https://doi.org/10.1038/nclimate2246>.
- Berry, D. I., and E. C. Kent, 2011: Air–sea fluxes from ICOADS: The construction of a new gridded dataset with uncertainty estimates. *Int. J. Climatol.*, **31**, 987–1001, <https://doi.org/10.1002/joc.2059>.
- Bindoff, N. L., and Coauthors, 2013: Detection and attribution of climate change: From global to regional. *Climate Change 2013: The Physical Science Basis*, T. F. Stocker et al., Eds., Cambridge University Press, 867–952.
- Blazquez, A., B. Meyssignac, J. M. Lemoine, E. Berthier, A. Ribes, and A. Cazenave, 2018: Exploring the uncertainty in GRACE estimates of the mass redistributions at the Earth surface: Implications for the global water and sea level budgets. *Geophys. J. Int.*, **215**, 415–430, <https://doi.org/10.1093/gji/ggy293>.
- Bojinski, S., M. Verstraete, T. C. Peterson, C. Richter, A. Simmons, and M. Zemp, 2014: The concept of essential climate variables in support of climate research, applications, and policy. *Bull. Amer. Meteor. Soc.*, **95**, 1431–1443, <https://doi.org/10.1175/BAMS-D-13-00047.1>.
- Bolch, T., L. Sandberg Sørensen, S. B. Simonsen, N. Mölg, H. Machguth, P. Rastner, and F. Paul, 2013: Mass loss of Greenland’s glaciers and ice caps 2003–2008 revealed from ICESat laser altimetry data. *Geophys. Res. Lett.*, **40**, 875–881, <https://doi.org/10.1002/grl.50270>.
- Bonfils, C. J. W., B. D. Santer, J. C. Fyfe, K. Marvel, T. J. Phillips, and S. R. H. Zimmerman, 2020: Human influence on joint changes in temperature, rainfall and continental aridity. *Nat. Climate Change*, **10**, 726–731, <https://doi.org/10.1038/s41558-020-0821-1>.
- Bosilovich, M. G., F. R. Robertson, L. Takacs, A. Molod, and D. Mocko, 2017: Atmospheric water balance and variability in the MERRA-2 reanalysis. *J. Climate*, **30**, 1177–1196, <https://doi.org/10.1175/JCLI-D-16-0338.1>.
- Böttcher, H., and Coauthors, 2017: Independent monitoring: Building trust and consensus around GHG data for increased accountability of mitigation in the land use sector. European Commission Rep., 112 pp., <https://doi.org/10.2834/513344>.
- Braithwaite, R. J., and P. D. Hughes, 2020: Regional geography of glacier mass balance variability over seven decades 1946–2015. *Front. Earth Sci.*, **8**, 302, <https://doi.org/10.3389/feart.2020.00302>.
- Brenninkmeijer, C. A. M., and Coauthors, 2007: Civil Aircraft for the Regular Investigation of the Atmosphere Based on an Instrumented Container: The new CARIBIC system. *Atmos. Chem. Phys.*, **7**, 4953–4976, <https://doi.org/10.5194/acp-7-4953-2007>.
- Broadbent, A. M., A. M. Coutts, K. A. Nice, M. Demuzere, E. S. Krayenhoff, N. J. Tapper, and H. Wouters, 2019: The Air-Temperature Response to Green/blue-infrastructure Evaluation Tool (TARGET v1.0): An efficient and user-friendly model of city cooling. *Geosci. Model Dev.*, **12**, 785–803, <https://doi.org/10.5194/gmd-12-785-2019>.
- Brocca, L., A. Tarpanelli, P. Filippucci, W. Dorigo, F. Zaussinger, A. Gruber, and D. Fernández-Prieto, 2018: How much water is used for irrigation? A new approach exploiting coarse resolution satellite soil moisture products. *Int. J. Appl. Earth Obs. Geoinf.*, **73**, 752–766, <https://doi.org/10.1016/j.jag.2018.08.023>.
- Brown, J., O. Ferrians, J. Heginbottom, and E. Melnikov, 2002: Circum-Arctic map of permafrost and ground-ice conditions, version 2. National Snow and Ice Data Center, accessed 9 August 2021, <https://nsidc.org/data/ggd318>.
- Brown, R. D., and C. Derksen, 2013: Is Eurasian October snow cover extent increasing? *Environ. Res. Lett.*, **8**, 024006, <https://doi.org/10.1088/1748-9326/8/2/024006>.
- , B. Fang, and L. Mudryk, 2019: Update of Canadian historical snow survey data and analysis of snow water equivalent trends, 1967–2016. *Atmos.–Ocean*, **57**, 149–156, <https://doi.org/10.1080/07055900.2019.1598843>.
- Burnett, W. C., M. Taniguchi, and J. Oberdorfer, 2001: Measurement and significance of the direct discharge of groundwater into the coastal zone. *J. Sea Res.*, **46**, 109–116, [https://doi.org/10.1016/S1385-1101\(01\)00075-2](https://doi.org/10.1016/S1385-1101(01)00075-2).
- Busker, T., A. de Roo, E. Gelati, C. Schwatke, M. Adamovic, B. Bisselink, J.-F. Pekel, and A. Cottam, 2019: A global lake and reservoir volume analysis using a surface water dataset and satellite altimetry. *Hydrol. Earth Syst. Sci.*, **23**, 669–690, <https://doi.org/10.5194/hess-23-669-2019>.
- Byrne, M. P., and P. A. O’Gorman, 2016: Understanding decreases in land relative humidity with global warming: Conceptual model and GCM simulations. *J. Climate*, **29**, 9045–9061, <https://doi.org/10.1175/JCLI-D-16-0351.1>.
- , and ———, 2018: Trends in continental temperature and humidity directly linked to ocean warming. *Proc. Natl. Acad. Sci. USA*, **115**, 4863–4868, <https://doi.org/10.1073/pnas.1722312115>.

- Cazenave, A., and Coauthors, 2018: Global sea-level budget 1993–present. *Earth Syst. Sci. Data*, **10**, 1551–1590, <https://doi.org/10.5194/essd-10-1551-2018>.
- Chang, A. T., J. L. Foster, and D. K. Hall, 1990: Satellite sensor estimates of Northern Hemisphere snow volume. *Int. J. Remote Sens.*, **11**, 167–171, <https://doi.org/10.1080/01431169008955009>.
- Chen, B., and Z. Liu, 2016: Global water vapor variability and trend from the latest 36 year (1979 to 2014) data of ECMWF and NCEP reanalyses, radiosonde, GPS, and microwave satellite. *J. Geophys. Res. Atmos.*, **121**, 11 442–11 462, <https://doi.org/10.1002/2016JD024917>.
- Chen, J., J. S. Famiglietti, B. R. Scanlon, and M. Rodell, 2016: Groundwater storage changes: Present status from GRACE observations. *Surv. Geophys.*, **37**, 397–417, <https://doi.org/10.1007/s10712-015-9332-4>.
- Cogley, J., and Coauthors, 2011: Glossary of glacier mass balance and related terms. IACS Contribution 2, 124 pp., <https://unesdoc.unesco.org/ark:/48223/pf0000192525>.
- Cook, B. I., J. S. Mankin, K. Marvel, A. P. Williams, J. E. Smerdon, and K. J. Anchukaitis, 2020a: Twenty-first century drought projections in the CMIP6 forcing scenarios. *Earth's Future*, **8**, e2019EF001461, <https://doi.org/10.1029/2019EF001461>.
- , S. S. McDermid, M. J. Puma, A. P. Williams, R. Seager, M. Kelley, L. Nazarenko, and I. Aleinov, 2020b: Divergent regional climate consequences of maintaining current irrigation rates in the 21st century. *J. Geophys. Res.*, **125**, e2019JD031814, <https://doi.org/10.1029/2019JD031814>.
- Crétaux, J. F., R. Abarca-del-Río, M. Bergé-Nguyen, A. Arsen, V. Drolon, G. Clos, and P. Maisongrande, 2016: Lake volume monitoring from space. *Surv. Geophys.*, **37**, 269–305, <https://doi.org/10.1007/s10712-016-9362-6>.
- de Graaf, I., E. H. Sutanudjaja, L. P. H. van Beek, and M. F. P. Bierkens, 2015: A high-resolution global-scale groundwater model. *Hydrol. Earth Syst. Sci.*, **19**, 823–837, <https://doi.org/10.5194/hess-19-823-2015>.
- , R. van Beek, T. Gleeson, N. Moosdorf, O. Schmitz, E. Sutanudjaja, and M. Bierkens, 2016: A global-scale two-layer transient groundwater model: Development and application to groundwater depletion. *Hydrol. Earth Syst. Sci. Discuss.*, <https://doi.org/10.5194/hess-2016-121>.
- Deines, J. M., A. D. Kendall, and D. W. Hyndman, 2017: Annual irrigation dynamics in the U.S. northern High Plains derived from Landsat satellite data. *Geophys. Res. Lett.*, **44**, 9350–9360, <https://doi.org/10.1002/2017GL074071>.
- Dillon, P., and Coauthors, 2019: Sixty years of global progress in managed aquifer recharge. *Hydrogeol. J.*, **27**, 1–30, <https://doi.org/10.1007/s10040-018-1841-z>.
- Dorigo, W. A., R. Richter, F. Baret, R. Bamler, and W. Wagner, 2009: Enhanced automated canopy characterization from hyperspectral data by a novel two step radiative transfer model inversion approach. *Remote Sens.*, **1**, 1139–1170, <https://doi.org/10.3390/rs1041139>.
- , K. Scipal, R. M. Parinussa, Y. Y. Liu, W. Wagner, R. A. M. de Jeu, and V. Naeimi, 2010: Error characterisation of global active and passive microwave soil moisture datasets. *Hydrol. Earth Syst. Sci.*, **14**, 2605–2616, <https://doi.org/10.5194/hess-14-2605-2010>.
- , and Coauthors, 2013: Global automated quality control of in situ soil moisture data from the International Soil Moisture Network. *Vadose Zone J.*, **12**, 1–21, <https://doi.org/10.2136/vzj2012.0097>.
- , and Coauthors, 2017: ESA CCI soil moisture for improved Earth system understanding: State-of-the art and future directions. *Remote Sens. Environ.*, **203**, 185–215, <https://doi.org/10.1016/j.rse.2017.07.001>.
- , I. Himmelbauer, L. Zappa, W. Preimesberger, D. Aberer, L. Schremmer, and I. Petrakovic, 2021: The International Soil Moisture Network: Serving Earth system science for over a decade. *Hydrol. Earth Syst. Sci. Discuss.*, <https://doi.org/10.5194/hess-2021-2>.
- Doughty, C. E., S. R. Loarie, and C. B. Field, 2012: Theoretical impact of changing albedo on precipitation at the southernmost boundary of the ITCZ in South America. *Earth Interact.*, **16**, <https://doi.org/10.1175/2012EI422.1>.
- Downing, J. A., and Coauthors, 2006: The global abundance and size distribution of lakes, ponds, and impoundments. *Limnol. Oceanogr.*, **51**, 2388–2397, <https://doi.org/10.4319/lo.2006.51.5.2388>.
- Droogers, P., W. W. Immerzeel, and I. J. Lorite, 2010: Estimating actual irrigation application by remotely sensed evapotranspiration observations. *Agric. Water Manage.*, **97**, 1351–1359, <https://doi.org/10.1016/j.agwat.2010.03.017>.
- Durack, P. J., and S. E. Wijffels, 2010: Fifty-year trends in global ocean salinities and their relationship to broad-scale warming. *J. Climate*, **23**, 4342–4362, <https://doi.org/10.1175/2010JCLI3377.1>.
- , ———, and R. J. Matear, 2012: Ocean salinities reveal strong global water cycle intensification during 1950 to 2000. *Science*, **336**, 455–458, <https://doi.org/10.1126/science.1212222>.
- Eakins, B. W., and G. F. Sharman, 2010: Volumes of the world's oceans from ETOPO1. NOAA National Geophys. Data Center, accessed 25 August 2020, www.ngdc.noaa.gov/mgg/global/etopo1_ocean_volumes.html.
- Edson, J. B., A. A. Hinton, K. E. Prada, J. E. Hare, and C. W. Fairall, 1998: Direct covariance flux estimates from mobile platforms at sea. *J. Atmos. Oceanic Technol.*, **15**, 547–562, [https://doi.org/10.1175/1520-0426\(1998\)015<0547:DCFEFM>2.0.CO;2](https://doi.org/10.1175/1520-0426(1998)015<0547:DCFEFM>2.0.CO;2).
- Eekhout, J. P. C., J. E. Hunink, W. Terink, and J. de Vente, 2018: Why increased extreme precipitation under climate change negatively affects water security. *Hydrol. Earth Syst. Sci.*, **22**, 5935–5946, <https://doi.org/10.5194/hess-22-5935-2018>.
- Elliott, G. W., 1974: Precipitation signatures in sea-surface-layer conditions during BOMEX. *J. Phys. Oceanogr.*, **4**, 498–501, [https://doi.org/10.1175/1520-0485\(1974\)004<0498:PSISLS>2.0.CO;2](https://doi.org/10.1175/1520-0485(1974)004<0498:PSISLS>2.0.CO;2).
- Ellison, D., and Coauthors, 2017: Trees, forests and water: Cool insights for a hot world. *Global Environ. Change*, **43**, 51–61, <https://doi.org/10.1016/j.gloenvcha.2017.01.002>.
- Enderlin, E. M., I. M. Howat, S. Jeong, M. J. Noh, J. H. Van Angelen, and M. R. Van Den Broeke, 2014: An improved mass budget for the Greenland ice sheet. *Geophys. Res. Lett.*, **41**, 866–872, <https://doi.org/10.1002/2013GL059010>.
- Entekhabi, D., and Coauthors, 2010: The Soil Moisture Active Passive (SMAP) mission. *Proc. IEEE*, **98**, 704–716, <https://doi.org/10.1109/JPROC.2010.2043918>.
- Fairall, C. W., and Coauthors, 2003: Bulk parameterization of air–sea fluxes: Updates and verification for the COARE algorithm. *J. Climate*, **16**, 571–591, [https://doi.org/10.1175/1520-0442\(2003\)016<0571:BPOASF>2.0.CO;2](https://doi.org/10.1175/1520-0442(2003)016<0571:BPOASF>2.0.CO;2).
- Famiglietti, J. S., 2014: The global groundwater crisis. *Nat. Climate Change*, **4**, 945–948, <https://doi.org/10.1038/nclimate2425>.
- FAO, 2021: AQUASTAT database. Accessed 19 August 2021, www.fao.org/nr/water/aquastat/data/query/index.html?lang=en.
- Farinotti, D., M. Huss, J. J. Fürst, J. Landmann, H. Machguth, F. Maussion, and A. Pandit, 2019: A consensus estimate for the ice thickness distribution of all glaciers on Earth. *Nat. Geosci.*, **12**, 168–173, <https://doi.org/10.1038/s41561-019-0300-3>.
- Fekete, B. M., C. J. Vörösmarty, and W. Grabs, 2002: High-resolution fields of global runoff combining observed river discharge and simulated water balances. *Global Biogeochem. Cycles*, **16**, 1042, <https://doi.org/10.1029/1999GB001254>.
- Ferreira, A. P., R. Nieto, and L. Gimeno, 2019: Completeness of radiosonde humidity observations based on the Integrated Global Radiosonde Archive. *Earth Syst. Sci. Data*, **11**, 603–627, <https://doi.org/10.5194/essd-11-603-2019>.
- Ferreira, V. G., and Z. Asiah, 2016: An investigation on the closure of the water budget methods over Volta basin using multi-satellite data. *International Association of Geodesy Symposia*, Vol. 144, Springer Verlag, 171–178.
- Fisher, J. B., and Coauthors, 2017: The future of evapotranspiration: Global requirements for ecosystem functioning, carbon and climate feedbacks, agricultural management, and water resources. *Water Resour. Res.*, **53**, 2618–2626, <https://doi.org/10.1002/2016WR020175>.
- Flörke, M., E. Kynast, I. Bärlund, S. Eisner, F. Wimmer, and J. Alcamo, 2013: Domestic and industrial water uses of the past 60 years as a mirror of socio-economic development: A global simulation study. *Global Environ. Change*, **23**, 144–156, <https://doi.org/10.1016/j.gloenvcha.2012.10.018>.
- Foley, J. A., and Coauthors, 2011: Solutions for a cultivated planet. *Nature*, **478**, 337–342, <https://doi.org/10.1038/nature10452>.
- Ford, T. W., E. Harris, and S. M. Quiring, 2014: Estimating root zone soil moisture using near-surface observations from SMOS. *Hydrol. Earth Syst. Sci.*, **18**, 139–154, <https://doi.org/10.5194/hess-18-139-2014>.

- Foster, S., J. Chilton, G. J. Nijsten, and A. Richts, 2013: Groundwater—A global focus on the “local resource.” *Curr. Opin. Environ. Sustain.*, **5**, 685–695, <https://doi.org/10.1016/j.cosust.2013.10.010>.
- Fowler, H. J., and Coauthors, 2021: Anthropogenic intensification of short-duration rainfall extremes. *Nat. Rev. Earth Environ.*, **2**, 107–122, <https://doi.org/10.1038/s43017-020-00128-6>.
- Frederikse, T., and Coauthors, 2020: The causes of sea-level rise since 1900. *Nature*, **584**, 393–397, <https://doi.org/10.1038/s41586-020-2591-3>.
- Gao, H., C. Birkett, and D. P. Lettenmaier, 2012: Global monitoring of large reservoir storage from satellite remote sensing. *Water Resour. Res.*, **48**, W09504, <https://doi.org/10.1029/2012WR012063>.
- Gardner, A. S., and Coauthors, 2013: A reconciled estimate of glacier contributions to sea level rise: 2003 to 2009. *Science*, **340**, 852–857, <https://doi.org/10.1126/science.1234532>.
- Gärtner-Roer, I., K. Naegeli, M. Huss, T. Knecht, H. Machguth, and M. Zemp, 2014: A database of worldwide glacier thickness observations. *Global Planet. Change*, **122**, 330–344, <https://doi.org/10.1016/j.gloplacha.2014.09.003>.
- GCOS, 2015: Status of the Global Observing System for Climate. WMO Rep., 353 pp., https://library.wmo.int/index.php?lvl=notice_display&id=18962.
- , 2016: The Global Observing System for Climate: Implementation needs. WMO Rep., 235 pp., <https://public.wmo.int/en/resources/library/global-observing-system-climate-implementation-needs>.
- Gedney, N., P. M. Cox, R. A. Betts, O. Boucher, C. Huntingford, and P. A. Stott, 2006: Detection of a direct carbon dioxide effect in continental river runoff records. *Nature*, **439**, 835–838, <https://doi.org/10.1038/nature04504>.
- Gentemann, C. L., and Coauthors, 2020: FluxSat: Measuring the ocean–atmosphere turbulent exchange of heat and moisture from space. *Remote Sens.*, **12**, 1796, <https://doi.org/10.3390/rs12111796>.
- Ghiggi, G., V. Humphrey, S. I. Seneviratne, and L. Gudmundsson, 2019: GRUN: An observation-based global gridded runoff dataset from 1902 to 2014. *Earth Syst. Sci. Data*, **11**, 1655–1674, <https://doi.org/10.5194/essd-11-1655-2019>.
- Gimeno, L., A. Drumond, R. Nieto, R. M. Trigo, and A. Stohl, 2010: On the origin of continental precipitation. *Geophys. Res. Lett.*, **37**, L13804, <https://doi.org/10.1029/2010GL043712>.
- , and Coauthors, 2012: Oceanic and terrestrial sources of continental precipitation. *Rev. Geophys.*, **50**, RG4003, <https://doi.org/10.1029/2012RG000389>.
- Gleeson, T., K. M. Befus, S. Jasechko, E. Luijendijk, and M. B. Cardenas, 2016: The global volume and distribution of modern groundwater. *Nat. Geosci.*, **9**, 161–167, <https://doi.org/10.1038/ngeo2590>.
- Gleick, P. H., 1996: Basic water requirements for human activities: Meeting basic needs. *Water Int.*, **21**, 83–92, <https://doi.org/10.1080/02508069608686494>.
- GLIMS and NSIDC, 2005: GLIMS glacier database, version 1 (updated 2018). National Snow and Ice Data Center, accessed 11 August 2021, <https://doi.org/DOI:10.7265/N5V98602>.
- Gonzalez, R. L., G. Liston, C. Chiu, and B. Notaros, 2019: Thesis consistency in the AMSR-E snow products: Groundwork for a coupled snowfall and SWE algorithm. M.S. thesis, Dept. of Atmospheric Science, Colorado State University, 60 pp., <https://mountainscholar.org/handle/10217/199801>.
- Goulden, M. L., and R. C. Bales, 2014: Mountain runoff vulnerability to increased evapotranspiration with vegetation expansion. *Proc. Natl. Acad. Sci. USA*, **111**, 14071–14075, <https://doi.org/10.1073/pnas.1319316111>.
- Gruber, A., W. A. Dorigo, S. Zwieback, A. Xaver, and W. Wagner, 2013: Characterizing coarse-scale representativeness of in situ soil moisture measurements from the International Soil Moisture Network. *Vadose Zone J.*, **12**, 1–16, <https://doi.org/10.2136/vzj2012.0170>.
- , T. Scanlon, R. van der Schalie, W. Wagner, and W. Dorigo, 2019: Evolution of the ESA CCI soil moisture climate data records and their underlying merging methodology. *Earth Syst. Sci. Data*, **11**, 717–739, <https://doi.org/10.5194/essd-11-717-2019>.
- Gutenstein, M., K. Fennig, M. Schröder, T. Trent, S. Bakan, J. B. Roberts, and F. R. Robertson, 2021: Intercomparison of freshwater fluxes over ocean and investigations into water budget closure. *Hydrol. Earth Syst. Sci.*, **25**, 121–146, <https://doi.org/10.5194/hess-25-121-2021>.
- Haberhorn, A., 2019: European snow booklet. COST Doc., 363 pp., <https://doi.org/10.16904/envidat.59>.
- Hamdi, R., and Coauthors, 2020: The state-of-the-art of urban climate change modeling and observations. *Earth Syst. Environ.*, **4**, 631–646, <https://doi.org/10.1007/s41748-020-00193-3>.
- Harris, I., P. D. Jones, T. J. Osborn, and D. H. Lister, 2014: Updated high-resolution grids of monthly climatic observations—The CRU TS3.10 dataset. *Int. J. Climatol.*, **34**, 623–642, <https://doi.org/10.1002/joc.3711>.
- Hegerl, G. C., and Coauthors, 2015: Challenges in quantifying changes in the global water cycle. *Bull. Amer. Meteor. Soc.*, **96**, 1097–1115, <https://doi.org/10.1175/BAMS-D-13-00212.1>.
- Hegglin, M. I., and Coauthors, 2013: SPARC data initiative: Comparison of water vapor climatologies from international satellite limb sounders. *J. Geophys. Res. Atmos.*, **118**, 11 824–11 846, <https://doi.org/10.1002/jgrd.50752>.
- Heginbottom, J. A., J. Brown, E. S. Melnikov, and O. J. Ferrians, Jr., 1993: Circum-Arctic map of permafrost and ground ice conditions. *Proc. Sixth Int. Conf. on Permafrost*, Beijing, China, Chinese Society of Glaciology and Geocryology, 1132–1136.
- Held, I. M., and B. J. Soden, 2006: Robust responses of the hydrological cycle to global warming. *J. Climate*, **19**, 5686–5699, <https://doi.org/10.1175/JCLI3990.1>.
- Herold, M., and Coauthors, 2019: The role and need for space-based forest biomass-related measurements in environmental management and policy. *Surv. Geophys.*, **40**, 757–778, <https://doi.org/10.1007/s10712-019-09510-6>.
- Hersbach, H., C. Peubey, A. Simmons, P. Berrisford, P. Poli, and D. Dee, 2015: ERA-20CM: A twentieth-century atmospheric model ensemble. *Quart. J. Roy. Meteor. Soc.*, **141**, 2350–2375, <https://doi.org/10.1002/qj.2528>.
- , and Coauthors, 2020: The ERA5 global reanalysis. *Quart. J. Roy. Meteor. Soc.*, **146**, 1999–2049, <https://doi.org/10.1002/qj.3803>.
- Heudorfer, B., E. Haaf, K. Stahl, and R. Barthel, 2019: Index-based characterization and quantification of groundwater dynamics. *Water Resour. Res.*, **55**, 5575–5592, <https://doi.org/10.1029/2018WR024418>.
- Hicks, F., and S. Beltaos, 2008: River ice. *Hydrologic Processes*, M.-k. Woo, Ed., Vol. 2, *Cold Region Atmospheric and Hydrologic Studies. The Mackenzie GEWEX Experience*, Springer, 281–305.
- Hirschi, M., and S. I. Seneviratne, 2017: Basin-scale water-balance dataset (BSWB): An update. *Earth Syst. Sci. Data*, **9**, 251–258, <https://doi.org/10.5194/essd-9-251-2017>.
- Hollmann, R., and Coauthors, 2013: The ESA climate change initiative: Satellite data records for essential climate variables. *Bull. Amer. Meteor. Soc.*, **94**, 1541–1552, <https://doi.org/10.1175/BAMS-D-11-00254.1>.
- Hosseini, M., and R. Kerachian, 2017: A data fusion-based methodology for optimal redesign of groundwater monitoring networks. *J. Hydrol.*, **552**, 267–282, <https://doi.org/10.1016/j.jhydrol.2017.06.046>.
- Hou, A. Y., and Coauthors, 2014: The Global Precipitation Measurement mission. *Bull. Amer. Meteor. Soc.*, **95**, 701–722, <https://doi.org/10.1175/BAMS-D-13-00164.1>.
- Huang, C., Y. Chen, S. Zhang, and J. Wu, 2018: Detecting, extracting, and monitoring surface water from space using optical sensors: A review. *Rev. Geophys.*, **56**, 333–360, <https://doi.org/10.1029/2018RG000598>.
- Huss, M., 2011: Present and future contribution of glacier storage change to runoff from macroscale drainage basins in Europe. *Water Resour. Res.*, **47**, W07511, <https://doi.org/10.1029/2010WR010299>.
- , 2013: Density assumptions for converting geodetic glacier volume change to mass change. *Cryosphere*, **7**, 877–887, <https://doi.org/10.5194/tc-7-877-2013>.
- , and R. Hock, 2015: A new model for global glacier change and sea-level rise. *Front. Earth Sci.*, **3**, 54, <https://doi.org/10.3389/feart.2015.00054>.
- Huuskonen, A., E. Saltikoff, and I. Holleman, 2014: The operational weather radar network in Europe. *Bull. Amer. Meteor. Soc.*, **95**, 897–907, <https://doi.org/10.1175/BAMS-D-12-00216.1>.
- Idso, S. B., and A. J. Brazel, 1984: Rising atmospheric carbon dioxide concentrations may increase streamflow. *Nature*, **312**, 51–53, <https://doi.org/10.1038/312051a0>.

- IPCC, 2019: *Special Report on the Ocean and Cryosphere in a Changing Climate*. IPCC, 765 pp., www.ipcc.ch/srocc/.
- Ishij, M., Y. Fukuda, S. Hirahara, S. Yasui, T. Suzuki, and K. Sato, 2017: Accuracy of global upper ocean heat content estimation expected from present observational data sets. *SOLA*, **13**, 163–167, <https://doi.org/10.2151/sola.2017-030>.
- Jackson, T. J., and T. J. Schugge, 1991: Vegetation effects on the microwave emission of soils. *Remote Sens. Environ.*, **36**, 203–212, [https://doi.org/10.1016/0034-4257\(91\)90057-D](https://doi.org/10.1016/0034-4257(91)90057-D).
- Jalilvand, E., M. Tajrishy, S. A. Ghazi Zadeh Hashemi, and L. Brocca, 2019: Quantification of irrigation water using remote sensing of soil moisture in a semi-arid region. *Remote Sens. Environ.*, **231**, 111226, <https://doi.org/10.1016/j.rse.2019.111226>.
- Jones, D. B., S. Harrison, K. Anderson, and R. A. Betts, 2018: Mountain rock glaciers contain globally significant water stores. *Sci. Rep.*, **8**, 2834, <https://doi.org/10.1038/s41598-018-21244-w>.
- , ———, ———, S. Shannon, and R. A. Betts, 2021: Rock glaciers represent hidden water stores in the Himalaya. *Sci. Total Environ.*, 145368, <https://doi.org/10.1016/j.scitotenv.2021.145368>, in press.
- Josey, S.A., E. C. Kent, and P.K. Taylor, 1999: New insights into the ocean heat budget closure problem from analysis of the SOC air–sea flux climatology. *J. Climate*, **12**, 2856–2880, [https://doi.org/10.1175/1520-0442\(1999\)012<2856:NIITOH>2.0.CO;2](https://doi.org/10.1175/1520-0442(1999)012<2856:NIITOH>2.0.CO;2).
- Jung, M., and Coauthors, 2019: The FLUXCOM ensemble of global land-atmosphere energy fluxes. *Sci. Data*, **6**, 74, <https://doi.org/10.1038/s41597-019-0076-8>.
- Kaser, G., M. Großhauser, and B. Marzeion, 2010: Contribution potential of glaciers to water availability in different climate regimes. *Proc. Natl. Acad. Sci. USA*, **107**, 20223–20227, <https://doi.org/10.1073/pnas.1008162107>.
- Kelly, R. E., A. T. Chang, L. Tsang, and J. L. Foster, 2003: A prototype AMSR-E global snow area and snow depth algorithm. *IEEE Trans. Geosci. Remote Sens.*, **41**, 230–242, <https://doi.org/10.1109/TGRS.2003.809118>.
- Kenway, S., A. Gregory, and J. McMahon, 2011: Urban water mass balance analysis. *J. Ind. Ecol.*, **15**, 693–706, <https://doi.org/10.1111/j.1530-9290.2011.00357.x>.
- Kerr, Y. H., and Coauthors, 2012: The SMOS soil moisture retrieval algorithm. *IEEE Trans. Geosci. Remote Sens.*, **50**, 1384–1403, <https://doi.org/10.1109/TGRS.2012.2184548>.
- Kidd, C., A. Becker, G. J. Huffman, C. L. Muller, P. Joe, G. Skofronick-Jackson, and D. B. Kirschbaum, 2017: So, how much of the Earth's surface is covered by rain gauges? *Bull. Amer. Meteor. Soc.*, **98**, 69–78, <https://doi.org/10.1175/BAMS-D-14-00283.1>.
- King, M. D., and Coauthors, 2020: Dynamic ice loss from the Greenland Ice Sheet driven by sustained glacier retreat. *Commun. Earth Environ.*, **1**, 1, <https://doi.org/10.1038/s43247-020-0001-2>.
- Kinzel, P., and C. Legleiter, 2019: sUAS-based remote sensing of river discharge using thermal particle image velocimetry and bathymetric lidar. *Remote Sens.*, **11**, 2317, <https://doi.org/10.3390/rs11192317>.
- Kittel, C. M. M., 2020: Satellite radar observations for hydrologic and hydrodynamic modelling. Ph.D. dissertation, Technical University of Denmark, 66 pp.
- Konikow, L. F., 2011: Contribution of global groundwater depletion since 1900 to sea-level rise. *Geophys. Res. Lett.*, **38**, L17401, <https://doi.org/10.1029/2011GL048604>.
- Konings, A. G., and M. Momen, 2018: Frequency-dependence of vegetation optical depth-derived isohydricity estimates. *Int. Geoscience and Remote Sensing Symp.*, Valencia, Spain, IEEE, 9045–9047, <https://doi.org/10.1109/IGARSS.2018.8519441>.
- Kooperman, G. J., M. D. Fowler, F. M. Hoffman, C. D. Koven, K. Lindsay, M. S. Pritchard, A. L. S. Swann, and J. T. Randerson, 2018: Plant physiological responses to rising CO₂ modify simulated daily runoff intensity with implications for global-scale flood risk assessment. *Geophys. Res. Lett.*, **45**, 12457–12466, <https://doi.org/10.1029/2018GL079901>.
- Koppa, A., S. Alam, D. G. Miralles, and M. Gebremichael, 2021, Budyko-based long-term water and energy balance closure in global watersheds from Earth observations. *Water Resour. Res.*, **57**, e2020WR028658, <https://doi.org/10.1029/2020WR028658>.
- Korzoun, V. I., and Coauthors, 1978: *World Water Balance and Water Resources of the Earth*. UNESCO Press, 663 pp.
- Koutsoyiannis, D., 2020: Revisiting the global hydrological cycle: Is it intensifying? *Hydrol. Earth Syst. Sci.*, **24**, 3899–3932, <https://doi.org/10.5194/hess-24-3899-2020>.
- Kumar, S. V., C. D. Peters-Lidard, J. A. Santanello, R. H. Reichle, C. S. Draper, R. D. Koster, G. Nearing, and M. F. Jasinski, 2015: Evaluating the utility of satellite soil moisture retrievals over irrigated areas and the ability of land data assimilation methods to correct for unmodeled processes. *Hydrol. Earth Syst. Sci.*, **19**, 4463–4478, <https://doi.org/10.5194/hess-19-4463-2015>.
- Landerer, F. W., J. O. Dickey, and A. Güntner, 2010: Terrestrial water budget of the Eurasian pan-Arctic from GRACE satellite measurements during 2003–2009. *J. Geophys. Res.*, **115**, D23115, <https://doi.org/10.1029/2010JD014584>.
- Landwehr, S., N. O'Sullivan, and B. Ward, 2015: Direct flux measurements from mobile platforms at sea: Motion and airflow distortion corrections revisited. *J. Atmos. Oceanic Technol.*, **32**, 1163–1178, <https://doi.org/10.1175/JTECH-D-14-00137.1>.
- Lawford, R. G., and Coauthors, 2004: Advancing global- and continental-scale hydrometeorology: Contributions of GEWEX hydrometeorology panel. *Bull. Amer. Meteor. Soc.*, **85**, 1917–1930, <https://doi.org/10.1175/BAMS-85-12-1917>.
- Lemordant, L., and P. Gentile, 2019: Vegetation response to rising CO₂ impacts extreme temperatures. *Geophys. Res. Lett.*, **46**, 1383–1392, <https://doi.org/10.1029/2018GL080238>.
- Levitus, S., and Coauthors, 2012: World ocean heat content and thermosteric sea level change (0–2000 m), 1955–2010. *Geophys. Res. Lett.*, **39**, L10603, <https://doi.org/10.1029/2012GL051106>.
- Li, B., and Coauthors, 2019: Global GRACE data assimilation for groundwater and drought monitoring: Advances and challenges. *Water Resour. Res.*, **55**, 7564–7586, <https://doi.org/10.1029/2018WR024618>.
- Lieven, H., and Coauthors, 2019: Snow depth variability in the Northern Hemisphere mountains observed from space. *Nat. Commun.*, **10**, 4629, <https://doi.org/10.1038/s41467-019-12566-y>.
- Liman, J., M. Schröder, K. Fennig, A. Andersson, and R. Hollmann, 2018: Uncertainty characterization of HOAPS 3.3 latent heat-flux-related parameters. *Atmos. Meas. Tech.*, **11**, 1793–1815, <https://doi.org/10.5194/amt-11-1793-2018>.
- Liu, W., and Coauthors, 2018: Investigating water budget dynamics in 18 river basins across the Tibetan Plateau through multiple datasets. *Hydrol. Earth Syst. Sci.*, **22**, 351–371, <https://doi.org/10.5194/hess-22-351-2018>.
- Liu, W. T., K. B. Katsaros, and J. A. Businger, 1979: Bulk parameterization of air-sea exchanges of heat and water vapor including the molecular constraints at the interface. *J. Atmos. Sci.*, **36**, 1722–1735, [https://doi.org/10.1175/1520-0469\(1979\)036<1722:BPOASE>2.0.CO;2](https://doi.org/10.1175/1520-0469(1979)036<1722:BPOASE>2.0.CO;2).
- Llovel, W., S. Purkey, B. Meyssignac, A. Blazquez, N. Kolodziejczyk, and J. Bamber, 2019: Global ocean freshening, ocean mass increase and global mean sea level rise over 2005–2015. *Sci. Rep.*, **9**, 17717, <https://doi.org/10.1038/s41598-019-54239-2>.
- Looser, U., I. Dornblut, and T. de Couet, 2007: The Global Terrestrial Network for River Discharge (GTN-R): Real-time access to river discharge data on a global scale. GRDC Rep. 36, 66 pp.
- Lopez, O., and Coauthors, 2020: Mapping groundwater abstractions from irrigated agriculture: Big data, inverse modeling and a satellite–model fusion approach. *Hydrol. Earth Syst. Sci.*, **24**, 5251–5277, <https://doi.org/10.5194/hess-24-5251-2020>.
- Luck, M., M. Landis, and F. Gassert, 2015: Aqueduct water stress projections: Decadal projections of water supply and demand using CMIP5 GCMs. World Resources Institute Tech. Note, 20 pp.
- Luijendijk, E., T. Gleeson, and N. Moosdorf, 2020: Fresh groundwater discharge insignificant for the world's oceans but important for coastal ecosystems. *Nat. Commun.*, **11**, 1260, <https://doi.org/10.1038/s41467-020-15064-8>.
- Luo, Z., Q. Shao, W. Wan, H. Li, X. Chen, S. Zhu, and X. Ding, 2021: A new method for assessing satellite-based hydrological data products using water budget closure. *J. Hydrol.*, **594**, 125927, <https://doi.org/10.1016/j.jhydrol.2020.125927>.

- Makihara, Y., 1996: A method for improving radar estimates of precipitation by comparing data from radars and raingauges. *J. Meteor. Soc. Japan*, **74**, 459–480, https://doi.org/10.2151/jmsj1965.74.4_459.
- Mariotti, A., M. V. Struglia, N. Zeng, and K. M. Lau, 2002: The hydrological cycle in the Mediterranean region and implications for the water budget of the Mediterranean Sea. *J. Climate*, **15**, 1674–1690, [https://doi.org/10.1175/1520-0442\(2002\)015<1674:THCITM>2.0.CO;2](https://doi.org/10.1175/1520-0442(2002)015<1674:THCITM>2.0.CO;2).
- Martens, B., and Coauthors, 2017: GLEAM v3: Satellite-based land evaporation and root-zone soil moisture. *Geosci. Model Dev.*, **10**, 1903–1925, <https://doi.org/10.5194/gmd-10-1903-2017>.
- , R. de Jeu, N. Verhoest, H. Schuurmans, J. Kleijer, and D. Miralles, 2018: Towards estimating land evaporation at field scales using GLEAM. *Remote Sens.*, **10**, 1720, <https://doi.org/10.3390/rs10111720>.
- Marvel, K., B. I. Cook, C. J. W. Bonfils, P. J. Durack, J. E. Smerdon, and A. P. Williams, 2019: Twentieth-century hydroclimate changes consistent with human influence. *Nature*, **569**, 59–65, <https://doi.org/10.1038/s41586-019-1149-8>.
- Massari, C., and Coauthors, 2020: A daily 25 km short-latency rainfall product for data-scarce regions based on the integration of the Global Precipitation Measurement mission rainfall and multiple-satellite soil moisture products. *Hydrol. Earth Syst. Sci.*, **24**, 2687–2710, <https://doi.org/10.5194/hess-24-2687-2020>.
- Masunaga, H., M. Schröder, F. A. Furuzawa, C. Kummerow, E. Rustemeier, and U. Schneider, 2019: Inter-product biases in global precipitation extremes. *Environ. Res. Lett.*, **14**, 125016, <https://doi.org/10.1088/1748-9326/ab5da9>.
- McCabe, M. F., A. Ershadi, C. Jimenez, D. G. Miralles, D. Michel, and E. F. Wood, 2016: The GEWEX LandFlux project: Evaluation of model evaporation using tower-based and globally gridded forcing data. *Geosci. Model Dev.*, **9**, 283–305, <https://doi.org/10.5194/gmd-9-283-2016>.
- , D. G. Miralles, T. R. H. Holmes, and J. B. Fisher, 2019: Advances in the remote sensing of terrestrial evaporation. *Remote Sens.*, **11**, 1138, <https://doi.org/10.3390/rs11091138>.
- Milliman, J. D., and K. L. Farnsworth, 2011: *River Discharge to the Coastal Ocean: A Global Synthesis*. Cambridge University Press, 384 pp.
- Miralles, D. G., R. A. M. De Jeu, J. H. Gash, T. R. H. Holmes, and A. J. Dolman, 2011: Magnitude and variability of land evaporation and its components at the global scale. *Hydrol. Earth Syst. Sci.*, **15**, 967–981, <https://doi.org/10.5194/hess-15-967-2011>.
- , and Coauthors, 2016: The WACMOS-ET project—Part 2: Evaluation of global terrestrial evaporation data sets. *Hydrol. Earth Syst. Sci.*, **20**, 823–842, <https://doi.org/10.5194/hess-20-823-2016>.
- , P. Gentile, S. I. Seneviratne, and A. J. Teuling, 2019: Land–atmospheric feedbacks during droughts and heatwaves: State of the science and current challenges. *Ann. N. Y. Acad. Sci.*, **1436**, 19–35, <https://doi.org/10.1111/nyas.13912>.
- Mitchell, A. L., A. Rosenqvist, and B. Mora, 2017: Current remote sensing approaches to monitoring forest degradation in support of countries measurement, reporting and verification (MRV) systems for REDD+. *Carbon Balance Manage.*, **12**, 9, <https://doi.org/10.1186/s13021-017-0078-9>.
- Moesinger, L., W. Dorigo, R. de Jeu, R. van der Schalie, T. Scanlon, I. Teubner, and M. Forkel, 2020: The global long-term microwave Vegetation Optical Depth Climate Archive (VODCA). *Earth Syst. Sci. Data*, **12**, 177–196, <https://doi.org/10.5194/essd-12-177-2020>.
- Mohan, C., A. W. Western, Y. Wei, and M. Saft, 2018: Predicting groundwater recharge for varying land cover and climate conditions—A global meta-study. *Hydrol. Earth Syst. Sci.*, **22**, 2689–2703, <https://doi.org/10.5194/hess-22-2689-2018>.
- Moholdt, G., B. Wouters, and A. S. Gardner, 2012: Recent mass changes of glaciers in the Russian High Arctic. *Geophys. Res. Lett.*, **39**, L10502, <https://doi.org/10.1029/2012GL051466>.
- Mokany, K., R. J. Raison, and A. S. Prokushkin, 2006: Critical analysis of root: Shoot ratios in terrestrial biomes. *Global Change Biol.*, **12**, 84–96, <https://doi.org/10.1111/j.1365-2486.2005.001043.x>.
- Moninger, W. R., S. G. Benjamin, B. D. Jamison, T. W. Schlatter, T. L. Smith, and E. J. Szoke, 2010: Evaluation of regional aircraft observations using TAMDAR. *Wea. Forecasting*, **25**, 627–645, <https://doi.org/10.1175/2009WAF2222321.1>.
- Moreira, A. A., A. L. Ruhoff, D. R. Roberti, V. de Arruda Souza, H. R. Rocha, and R. C. D. de Paiva, 2019: Assessment of terrestrial water balance using remote sensing data in South America. *J. Hydrol.*, **575**, 131–147, <https://doi.org/10.1016/j.jhydrol.2019.05.021>.
- Morrow, R., and Coauthors, 2019: Global observations of fine-scale ocean surface topography with the Surface Water and Ocean Topography (SWOT) mission. *Front. Mar. Sci.*, **6**, 232, <https://doi.org/10.3389/fmars.2019.00232>.
- Mortimer, C., L. Mudryk, C. Derksen, K. Luoju, R. Brown, R. Kelly, and M. Tedesco, 2020: Evaluation of long-term Northern Hemisphere snow water equivalent products. *Cryosphere*, **14**, 1579–1594, <https://doi.org/10.5194/tc-14-1579-2020>.
- Munier, S., and F. Aires, 2018: A new global method of satellite dataset merging and quality characterization constrained by the terrestrial water budget. *Remote Sens. Environ.*, **205**, 119–130, <https://doi.org/10.1016/j.rse.2017.11.008>.
- , ———, S. Schläffer, C. Prigent, F. Papa, P. Maisongrande, and M. Pan, 2014: Combining data sets of satellite-retrieved products for basin-scale water balance study: 2. Evaluation on the Mississippi basin and closure correction model. *J. Geophys. Res. Atmos.*, **119**, 12 100–12 116, <https://doi.org/10.1002/2014JD021953>.
- National Academies of Sciences, Engineering, and Medicine, 2016: *Attribution of Extreme Weather Events in the Context of Climate Change*. National Academies Press, 186 pp.
- Ning, S., H. Ishidaira, and J. Wang, 2014: Statistical downscaling of grace-derived terrestrial water storage using satellite and GLDAS products. *Ann. J. Hydraul. Eng.*, **70**, 133–138, https://doi.org/10.2208/jsejhe.70.1_133.
- Oki, T., 1999: The global water cycle. *Global Energy and Water Cycles*, K. A. Browning and R. J. Gurney, Eds., Cambridge University Press, 10–27.
- , and S. Kanae, 2006: Global hydrological cycles and world water resources. *Science*, **313**, 1068–1072, <https://doi.org/10.1126/science.1128845>.
- Padrón, R. S., and Coauthors, 2020: Observed changes in dry-season water availability attributed to human-induced climate change. *Nat. Geosci.*, **13**, 477–481, <https://doi.org/10.1038/s41561-020-0594-1>.
- Pan, M., and E. F. Wood, 2006: Data assimilation for estimating the terrestrial water budget using a constrained ensemble Kalman filter. *J. Hydrometeorol.*, **7**, 534–547, <https://doi.org/10.1175/JHM495.1>.
- , A. K. Sahoo, T. J. Troy, R. K. Vinukollu, J. Sheffield, and A. E. F. Wood, 2012: Multisource estimation of long-term terrestrial water budget for major global river basins. *J. Climate*, **25**, 3191–3206, <https://doi.org/10.1175/JCLI-D-11-00300.1>.
- Pan, S., and Coauthors, 2020: Evaluation of global terrestrial evapotranspiration using state-of-the-art approaches in remote sensing, machine learning and land surface modeling. *Hydrol. Earth Syst. Sci.*, **24**, 1485–1509, <https://doi.org/10.5194/hess-24-1485-2020>.
- Paul, F., and Coauthors, 2009: Recommendations for the compilation of glacier inventory data from digital sources. *Ann. Glaciol.*, **50**, 119–126, <https://doi.org/10.3189/172756410790595778>.
- Pellarin, T., and Coauthors, 2020: The Precipitation Inferred from Soil Moisture (PrISM) near real-time rainfall product: Evaluation and comparison. *Remote Sens.*, **12**, 481, <https://doi.org/10.3390/rs12030481>.
- Pellet, V., F. Aires, S. Munier, D. Fernández Prieto, G. Jordá, W. A. Dorigo, J. Polcher, and L. Brocca, 2019: Integrating multiple satellite observations into a coherent dataset to monitor the full water cycle—Application to the Mediterranean region. *Hydrol. Earth Syst. Sci.*, **23**, 465–491, <https://doi.org/10.5194/hess-23-465-2019>.
- , ———, F. Papa, S. Munier, and B. Decharme, 2020: Long-term total water storage change from a satellite water cycle reconstruction over large southern Asian basins. *Hydrol. Earth Syst. Sci.*, **24**, 3033–3055, <https://doi.org/10.5194/hess-24-3033-2020>.
- Peña-Arancibia, J. L., L. A. Bruijnzeel, M. Mulligan, and A. I. J. M. van Dijk, 2019: Forests as ‘sponges’ and ‘pumps’: Assessing the impact of deforestation on dry-season flows across the tropics. *J. Hydrol.*, **574**, 946–963, <https://doi.org/10.1016/j.jhydrol.2019.04.064>.

- Penman, J., and Coauthors, 2003: Good practice guidance for land use, land-use change and forestry. IPCC Rep., 590 pp.
- Petersen, W., and Coauthors, 2016: GPM level 1 science requirements: Science and performance viewed from the ground. NASA Doc., 1 p., <https://ntrs.nasa.gov/citations/20160012025>.
- Petzold, A., and Coauthors, 2015: Global-scale atmosphere monitoring by in-service aircraft—Current achievements and future prospects of the European Research Infrastructure IAGOS. *Tellus*, **67B**, 28452, <https://doi.org/10.3402/tellusb.v67.28452>.
- Pfahl, S., P. A. O’Gorman, and E. M. Fischer, 2017: Understanding the regional pattern of projected future changes in extreme precipitation. *Nat. Climate Change*, **7**, 423–427, <https://doi.org/10.1038/nclimate3287>.
- Popp, T., and Coauthors, 2020: Consistency of satellite climate data records for Earth system monitoring. *Bull. Amer. Meteor. Soc.*, **101**, E1948–E1971, <https://doi.org/10.1175/BAMS-D-19-0127.1>.
- Preimesberger, W., T. Scanlon, C.-H. Su, A. Gruber, and W. Dorigo, 2020: Homogenization of structural breaks in the global ESA CCI soil moisture multisatellite climate data record. *IEEE Trans. Geosci. Remote Sens.*, **59**, 2845–2862, <https://doi.org/10.1109/TGRS.2020.3012896>.
- Pritchard, H. D., 2019: Asia’s shrinking glaciers protect large populations from drought stress. *Nature*, **569**, 649–654, <https://doi.org/10.1038/s41586-019-1240-1>.
- Prytherch, J., E. C. Kent, S. Fangohr, and D. I. Berry, 2015: A comparison of SSM/I-derived global marine surface-specific humidity datasets. *Int. J. Climatol.*, **35**, 2359–2381, <https://doi.org/10.1002/joc.4150>.
- Pulliainen, J., 2006: Mapping of snow water equivalent and snow depth in boreal and sub-Arctic zones by assimilating space-borne microwave radiometer data and ground-based observations. *Remote Sens. Environ.*, **101**, 257–269, <https://doi.org/10.1016/j.rse.2006.01.002>.
- , and Coauthors, 2020: Patterns and trends of Northern Hemisphere snow mass from 1980 to 2018. *Nature*, **581**, 294–298, <https://doi.org/10.1038/s41586-020-2258-0>.
- Raj, R. P., and Coauthors, 2020: Arctic sea level budget assessment during the GRACE/Argo time period. *Remote Sens.*, **12**, 2837, <https://doi.org/10.3390/rs12172837>.
- Rast, M., J. Johannessen, and W. Mauser, 2014: Review of understanding of Earth’s hydrological cycle: Observations, theory and modelling. *Surv. Geophys.*, **35**, 491–513, <https://doi.org/10.1007/s10712-014-9279-x>.
- Reinecke, R., L. Foglia, S. Mehl, T. Trautmann, D. Cáceres, and P. Döll, 2019: Challenges in developing a global gradient-based groundwater model (G³M v1.0) for the integration into a global hydrological model. *Geosci. Model Dev.*, **12**, 2401–2418, <https://doi.org/10.5194/gmd-12-2401-2019>.
- Reul, N., and Coauthors, 2020: Sea surface salinity estimates from space-borne L-band radiometers: An overview of the first decade of observation (2010–2019). *Remote Sens. Environ.*, **242**, 111769, <https://doi.org/10.1016/j.rse.2020.111769>.
- RGI, 2017: Randolph Glacier Inventory 6.0. RGI Tech. Rep., 71 pp., <https://doi.org/10.7265/n5-rgi-60>.
- Robertson, F. R., and Coauthors, 2020: Uncertainties in ocean latent heat flux variations over recent decades in satellite-based estimates and reduced observation reanalyses. *J. Climate*, **33**, 8415–8437, <https://doi.org/10.1175/JCLI-D-19-0954.1>.
- Robock, A., K. Y. Vinnikov, G. Srinivasan, J. K. Entin, S. E. Hollinger, N. A. Speranskaya, S. Liu, and A. Namkhaj, 2000: The Global Soil Moisture Data Bank. *Bull. Amer. Meteor. Soc.*, **81**, 1281–1299, [https://doi.org/10.1175/1520-0477\(2000\)081<1281:TGSMDB>2.3.CO;2](https://doi.org/10.1175/1520-0477(2000)081<1281:TGSMDB>2.3.CO;2).
- Rodell, M., J. S. Famiglietti, J. Chen, S. I. Seneviratne, P. Viterbo, S. Holl, and C. R. Wilson, 2004: Basin scale estimates of evapotranspiration using GRACE and other observations. *Geophys. Res. Lett.*, **31**, L20504, <https://doi.org/10.1029/2004GL020873>.
- , E. B. McWilliams, J. S. Famiglietti, H. K. Beaudoin, and J. Nigro, 2011: Estimating evapotranspiration using an observation based terrestrial water budget. *Hydrol. Processes*, **25**, 4082–4092, <https://doi.org/10.1002/hyp.8369>.
- , and Coauthors, 2015: The observed state of the water cycle in the early twenty-first century. *J. Climate*, **28**, 8289–8318, <https://doi.org/10.1175/JCLI-D-14-00555.1>.
- , J. S. Famiglietti, D. N. Wiese, J. T. Reager, H. K. Beaudoin, F. W. Landerer, and M. H. Lo, 2018: Emerging trends in global freshwater availability. *Nature*, **557**, 651–659, <https://doi.org/10.1038/s41586-018-0123-1>.
- Sadat-Noori, M., I. R. Santos, C. J. Sanders, L. M. Sanders, and D. T. Maher, 2015: Groundwater discharge into an estuary using spatially distributed radon time series and radium isotopes. *J. Hydrol.*, **528**, 703–719, <https://doi.org/10.1016/j.jhydrol.2015.06.056>.
- Sahely, H. R., S. Dudding, and C. A. Kennedy, 2003: Estimating the urban metabolism of Canadian cities: Greater Toronto area case study. *Can. J. Civ. Eng.*, **30**, 468–483, <https://doi.org/10.1139/l02-105>.
- Sahoo, A. K., M. Pan, T. J. Troy, R. K. Vinukollu, J. Sheffield, and E. F. Wood, 2011: Reconciling the global terrestrial water budget using satellite remote sensing. *Remote Sens. Environ.*, **115**, 1850–1865, <https://doi.org/10.1016/j.rse.2011.03.009>.
- Saltikoff, E., and Coauthors, 2019: An overview of using weather radar for climatological studies successes, challenges, and potential. *Bull. Amer. Meteor. Soc.*, **100**, 1739–1752, <https://doi.org/10.1175/BAMS-D-18-0166.1>.
- Schmied, H. M., and Coauthors, 2021: The global water resources and use model WaterGAP v2.2d: Model description and evaluation. *Geosci. Model Dev.*, **14**, 1037–1079, <https://doi.org/10.5194/gmd-14-1037-2021>.
- Schmitt, R. W., 1995: The ocean component of the global water cycle. *Rev. Geophys.*, **33**, 1395–1409, <https://doi.org/10.1029/95RG00184>.
- Schneider, U., A. Becker, P. Finger, A. Meyer-Christoffer, M. Ziese, and B. Rudolf, 2014: GPCP’s new land surface precipitation climatology based on quality-controlled in situ data and its role in quantifying the global water cycle. *Theor. Appl. Climatol.*, **115**, 15–40, <https://doi.org/10.1007/s00704-013-0860-x>.
- , P. Finger, A. Meyer-Christoffer, E. Rustemeier, M. Ziese, and A. Becker, 2017: Evaluating the hydrological cycle over land using the newly-corrected precipitation climatology from the Global Precipitation Climatology Centre (GPCC). *Atmosphere*, **8**, 52, <https://doi.org/10.3390/atmos8030052>.
- Schröder, M., M. Lockhoff, J. M. Forsythe, H. Q. Cronk, T. H. Vonder Haar, and R. Bennartz, 2016: The GEWEX water vapor assessment: Results from inter-comparison, trend, and homogeneity analysis of total column water vapor. *J. Appl. Meteor. Climatol.*, **55**, 1633–1649, <https://doi.org/10.1175/JAMC-D-15-0304.1>.
- Seneviratne, S. I., T. Corti, E. L. Davin, M. Hirschi, E. B. Jaeger, I. Lehner, B. Orlowsky, and A. J. Teuling, 2010: Investigating soil moisture-climate interactions in a changing climate: A review. *Earth-Sci. Rev.*, **99**, 125–161, <https://doi.org/10.1016/j.earscirev.2010.02.004>.
- Sheffield, J., C. R. Ferguson, T. J. Troy, E. F. Wood, and M. F. McCabe, 2009: Closing the terrestrial water budget from satellite remote sensing. *Geophys. Res. Lett.*, **36**, L07403, <https://doi.org/10.1029/2009GL037338>.
- Shepherd, A., and Coauthors, 2018: Mass balance of the Antarctic ice sheet from 1992 to 2017. *Nature*, **558**, 219–222, <https://doi.org/10.1038/s41586-018-0179-y>.
- , and Coauthors, 2020: Mass balance of the Greenland ice sheet from 1992 to 2018. *Nature*, **579**, 233–239, <https://doi.org/10.1038/s41586-019-1855-2>.
- Shige, S., and C. D. Kummerow, 2016: Precipitation-top heights of heavy orographic rainfall in the Asian monsoon region. *J. Atmos. Sci.*, **73**, 3009–3024, <https://doi.org/10.1175/JAS-D-15-0271.1>.
- Shiklomanov, I. A., 2000: Appraisal and assessment of world water resources. *Water Int.*, **25**, 11–32, <https://doi.org/10.1080/02508060008686794>.
- , 2008: *Water Resources of Russia and Their Use*. GGI, 600 pp.
- , and J. Rodda, 2004: World water resources at the beginning of the twenty-first century. *Choice Rev. Online*, **41**, 4063–4063, <https://doi.org/10.5860/CHOICE.41-4063>.
- , S. Déry, M. Tretiakov, D. Yang, D. Magritsky, A. Georgiadi, and W. Tang, 2021: River freshwater flux to the Arctic Ocean. *Arctic Hydrology, Permafrost and Ecosystems*, Springer International Publishing, 703–738.

- Siebert, S., and P. Döll, 2010: Quantifying blue and green virtual water contents in global crop production as well as potential production losses without irrigation. *J. Hydrol.*, **384**, 198–217, <https://doi.org/10.1016/j.jhydrol.2009.07.031>.
- Singh, P., and L. Bengtsson, 2004: Hydrological sensitivity of a large Himalayan basin to climate change. *Hydrol. Processes*, **18**, 2363–2385, <https://doi.org/10.1002/hyp.1468>.
- Slater, T., A. E. Hogg, and R. Mottram, 2020: Ice-sheet losses track high-end sea-level rise projections. *Nat. Climate Change*, **10**, 879–881, <https://doi.org/10.1038/s41558-020-0893-y>.
- Spawn, S. A., C. C. Sullivan, T. J. Lark, and H. K. Gibbs, 2020: Harmonized global maps of above and belowground biomass carbon density in the year 2010. *Sci. Data*, **7**, 112, <https://doi.org/10.1038/s41597-020-0444-4>.
- Srinivasamoorthy, K., G. Ponnunani, R. Prakash, S. Gopinath, K. Saravanan, and F. Vinnarasi, 2019: Tracing groundwater inputs to Bay of Bengal from Sankarabarani River basin, Pondicherry, India, using continuous radon monitoring. *Int. J. Environ. Sci. Technol.*, **16**, 5513–5524, <https://doi.org/10.1007/s13762-018-1938-x>.
- Stefan, C., and N. Ansems, 2018: Web-based global inventory of managed aquifer recharge applications. *Sustain. Water Resour. Manage.*, **4**, 153–162, <https://doi.org/10.1007/s40899-017-0212-6>.
- Stephens, G. L., and Coauthors, 2012: An update on Earth's energy balance in light of the latest global observations. *Nat. Geosci.*, **5**, 691–696, <https://doi.org/10.1038/ngeo1580>.
- Stickler, A., and Coauthors, 2010: The Comprehensive Historical Upper-Air Network. *Bull. Amer. Meteor. Soc.*, **91**, 741–752, <https://doi.org/10.1175/2009BAMS2852.1>.
- Swenson, S., and J. Wahr, 2009: Monitoring the water balance of Lake Victoria, East Africa, from space. *J. Hydrol.*, **370**, 163–176, <https://doi.org/10.1016/j.jhydrol.2009.03.008>.
- Syed, T. H., J. S. Famiglietti, V. Zlotnicki, and M. Rodell, 2007: Contemporary estimates of pan-Arctic freshwater discharge from GRACE and reanalysis. *Geophys. Res. Lett.*, **34**, L19404, <https://doi.org/10.1029/2007GL031254>.
- Szeto, K. K., 2007: Assessing water and energy budgets for the Saskatchewan River basin. *J. Meteor. Soc. Japan*, **85A**, 167–186, <https://doi.org/10.2151/jmsj.85A.167>.
- , R. E. Stewart, M. K. Yau, and J. Gyakum, 2008: The Mackenzie climate system: A synthesis of MAGS atmospheric research. *Atmospheric Dynamics, M.-k. Woo, Ed., Vol. 1, Cold Region Atmospheric and Hydrologic Studies. The Mackenzie GEWEX Experience*, Springer, 23–50.
- Takala, M., K. Luojus, J. Pulliainen, C. Derksen, J. Lemmetyinen, J. P. Kärnä, J. Koskinen, and B. Bojkov, 2011: Estimating Northern Hemisphere snow water equivalent for climate research through assimilation of space-borne radiometer data and ground-based measurements. *Remote Sens. Environ.*, **115**, 3517–3529, <https://doi.org/10.1016/j.rse.2011.08.014>.
- , J. Ikonen, K. Luojus, J. Lemmetyinen, S. Metsamaki, J. Cohen, A. N. Arslan, and J. Pulliainen, 2017: New snow water equivalent processing system with improved resolution over Europe and its applications in hydrology. *IEEE J. Sel. Top. Appl. Earth Obs. Remote Sens.*, **10**, 428–436, <https://doi.org/10.1109/JSTARS.2016.2586179>.
- Talsma, C. J., S. P. Good, C. Jimenez, B. Martens, J. B. Fisher, D. G. Miralles, M. F. McCabe, and A. J. Purdy, 2018: Partitioning of evapotranspiration in remote sensing-based models. *Agric. For. Meteorol.*, **260–261**, 131–143, <https://doi.org/10.1016/j.agrformet.2018.05.010>.
- Tarek, M., F. P. Brissette, and R. Arsenault, 2020: Evaluation of the ERA5 reanalysis as a potential reference dataset for hydrological modelling over North America. *Hydrol. Earth Syst. Sci.*, **24**, 2527–2544, <https://doi.org/10.5194/hess-24-2527-2020>.
- Taylor, R. G., and Coauthors, 2013: Ground water and climate change. *Nat. Climate Change*, **3**, 322–329, <https://doi.org/10.1038/nclimate1744>.
- Thomas, B., A. Behrangi, and J. Famiglietti, 2016: Precipitation intensity effects on groundwater recharge in the southwestern United States. *Water*, **8**, 90, <https://doi.org/10.3390/w8030090>.
- Thomas, C. M., B. Dong, and K. Haines, 2020: Inverse modeling of global and regional energy and water cycle fluxes using Earth observation data. *J. Climate*, **33**, 1707–1723, <https://doi.org/10.1175/JCLI-D-19-0343.1>.
- Tong, X., and Coauthors, 2020: Forest management in southern China generates short term extensive carbon sequestration. *Nat. Commun.*, **11**, 129, <https://doi.org/10.1038/s41467-019-13798-8>.
- Treichler, D., and A. Kääb, 2016: ICESat laser altimetry over small mountain glaciers. *Cryosphere*, **10**, 2129–2146, <https://doi.org/10.5194/tc-10-2129-2016>.
- Trenberth, K. E., and J. T. Fasullo, 2013: An apparent hiatus in global warming? *Earth's Future*, **1**, 19–32, <https://doi.org/10.1002/2013EF000165>.
- , L. Smith, T. Qian, A. Dai, and J. Fasullo, 2007: Estimates of the global water budget and its annual cycle using observational and model data. *J. Hydrometeorol.*, **8**, 758–769, <https://doi.org/10.1175/JHM600.1>.
- , J. T. Fasullo, and J. Mackaro, 2011: Atmospheric moisture transports from ocean to land and global energy flows in reanalyses. *J. Climate*, **24**, 4907–4924, <https://doi.org/10.1175/2011JCLI4171.1>.
- Ukkola, A. M., I. C. Prentice, T. F. Keenan, A. I. J. M. Van Dijk, N. R. Viney, R. B. Myneni, and J. Bi, 2016: Reduced streamflow in water-stressed climates consistent with CO₂ effects on vegetation. *Nat. Climate Change*, **6**, 75–78, <https://doi.org/10.1038/nclimate2831>.
- UNESCO, 2020: World Water Development Report 2020: Water and climate change. UNESCO Rep., 234 pp.
- United Nations, 2015: Adoption of the Paris Agreement. UN Doc., 27 pp.
- van der Ent, R. J., and O. A. Tuinenburg, 2017: The residence time of water in the atmosphere revisited. *Hydrol. Earth Syst. Sci.*, **21**, 779–790, <https://doi.org/10.5194/hess-21-779-2017>.
- van Dijk, A. I. J. M., J. Schellekens, M. Yebra, H. E. Beck, L. J. Renzullo, A. Weerts, and G. Donchyts, 2018: Global 5 km resolution estimates of secondary evaporation including irrigation through satellite data assimilation. *Hydrol. Earth Syst. Sci.*, **22**, 4959–4980, <https://doi.org/10.5194/hess-22-4959-2018>.
- Vicente-Serrano, S. M., T. R. McVicar, D. G. Miralles, Y. Yang, and M. Tomas-Burguera, 2020: Unraveling the influence of atmospheric evaporative demand on drought and its response to climate change. *Wiley Interdiscip. Rev.: Climate Change*, **11**, <https://doi.org/10.1002/wcc.632>.
- Vinogradova, N., and Coauthors, 2019: Satellite salinity observing system: Recent discoveries and the way forward. *Front. Mar. Sci.*, **6**, 243, <https://doi.org/10.3389/fmars.2019.00243>.
- Voss, K. A., J. S. Famiglietti, M. Lo, C. De Linage, M. Rodell, and S. C. Swenson, 2013: Groundwater depletion in the Middle East from GRACE with implications for transboundary water management in the Tigris-Euphrates-western Iran region. *Water Resour. Res.*, **49**, 904–914, <https://doi.org/10.1002/wrcr.20078>.
- Wada, Y., L. P. H. Van Beek, and M. F. P. Bierkens, 2012: Nonsustainable groundwater sustaining irrigation: A global assessment. *Water Resour. Res.*, **48**, W00L06, <https://doi.org/10.1029/2011WR010562>.
- , D. Wisser, and M. F. P. Bierkens, 2014: Global modeling of withdrawal, allocation and consumptive use of surface water and groundwater resources. *Earth Syst. Dyn.*, **5**, 15–40, <https://doi.org/10.5194/esd-5-15-2014>.
- Wagner, W., and Coauthors, 2013: The ASCAT soil moisture product: A review of its specifications, validation results, and emerging applications. *Meteor. Z.*, **22**, 5–33, <https://doi.org/10.1127/0941-2948/2013/0399>.
- Wang, J., and L. Zhang, 2008: Systematic errors in global radiosonde precipitable water data from comparisons with ground-based GPS measurements. *J. Climate*, **21**, 2218–2238, <https://doi.org/10.1175/2007JCLI1944.1>.
- Wang, S., D. W. McKenney, J. Shang, and J. Li, 2014: A national-scale assessment of long-term water budget closures for Canada's watersheds. *J. Geophys. Res.*, **119**, 8712–8725, <https://doi.org/10.1002/2014JD021951>.
- , J. Huang, D. Yang, G. Pavlic, and J. Li, 2015: Long-term water budget imbalances and error sources for cold region drainage basins. *Hydrol. Processes*, **29**, 2125–2136, <https://doi.org/10.1002/hyp.10343>.
- Weber, M., L. Braun, W. Mauser, and M. Prasch, 2010: Contribution of rain, snow- and icemelt in the upper Danube discharge today and in the future. *Geogr. Fis. Din. Quat.*, **332**, 221–230.

- Welty, E., and Coauthors, 2020: Worldwide version-controlled database of glacier thickness observations. *Earth Syst. Sci. Data*, **12**, 3039–3055, <https://doi.org/10.5194/essd-12-3039-2020>.
- Whitcher, B., S. D. Byers, P. Guttorp, and D. B. Percival, 2002: Testing for homogeneity of variance in time series: Long memory, wavelets, and the Nile River. *Water Resour. Res.*, **38**, 1054, <https://doi.org/10.1029/2001WR000509>.
- Wickert, J., and Coauthors, 2001: Atmosphere sounding by GPS radio occultation: First results from CHAMP. *Geophys. Res. Lett.*, **28**, 3263–3266, <https://doi.org/10.1029/2001GL013117>.
- Willett, K. M., R. J. H. Dunn, J. J. Kennedy, and D. I. Berry, 2020: Development of the HadISDH.marine humidity climate monitoring dataset. *Earth Syst. Sci. Data*, **12**, 2853–2880, <https://doi.org/10.5194/essd-12-2853-2020>.
- Williams, A. P., and Coauthors, 2020: Large contribution from anthropogenic warming to an emerging North American megadrought. *Science*, **368**, 314–318, <https://doi.org/10.1126/science.aaz9600>.
- Williamson, C. E., J. E. Saros, W. F. Vincent, and J. P. Smol, 2009: Lakes and reservoirs as sentinels, integrators, and regulators of climate change. *Limnol. Oceanogr.*, **54**, 2273–2282, https://doi.org/10.4319/lo.2009.54.6_part_2.2273.
- WMO, 2008: *Hydrology—From Measurement to Hydrological Information*. Vol. I, *Guide to Hydrological Practices*, WMO, 296 pp.
- Wouters, B., A. S. Gardner, and G. Moholdt, 2019: Global glacier mass loss during the GRACE satellite mission (2002–2016). *Front. Earth Sci.*, **7**, 96, <https://doi.org/10.3389/feart.2019.00096>.
- WUADAPT, 2020: World Urban Database: World Urban Database and Access Portal Tools. Accessed 8 October 2020, www.wudapt.org/.
- Yang, H., C. Huntingford, A. Wiltshire, S. Sitch, and L. Mercado, 2019: Compensatory climate effects link trends in global runoff to rising atmospheric CO₂ concentration. *Environ. Res. Lett.*, **14**, 124075, <https://doi.org/10.1088/1748-9326/ab5c6f>.
- Yeber, M., X. Quan, D. Riaño, P. Rozas Larraondo, A. I. J. M. van Dijk, and G. J. Cary, 2018: A fuel moisture content and flammability monitoring methodology for continental Australia based on optical remote sensing. *Remote Sens. Environ.*, **212**, 260–272, <https://doi.org/10.1016/j.rse.2018.04.053>.
- Yin, J., X. Zhan, J. Liu, and M. Schull, 2019: An intercomparison of Noah model skills with benefits of assimilating SMOPS blended and individual soil moisture retrievals. *Water Resour. Res.*, **55**, 2572–2592, <https://doi.org/10.1029/2018WR024326>.
- Yu, L., X. Jin, S. A. Josey, T. Lee, A. Kumar, C. Wen, and Y. Xue, 2017: The global ocean water cycle in atmospheric reanalysis, satellite, and ocean salinity. *J. Climate*, **30**, 3829–3852, <https://doi.org/10.1175/JCLI-D-16-0479.1>.
- , S. A. Josey, F. M. Bingham, and T. Lee, 2020: Intensification of the global water cycle and evidence from ocean salinity: A synthesis review. *Ann. N. Y. Acad. Sci.*, **1472**, 76–94, <https://doi.org/10.1111/nyas.14354>.
- Zaussinger, F., W. Dorigo, A. Gruber, A. Tarpanelli, P. Filippucci, and L. Brocca, 2019: Estimating irrigation water use over the contiguous United States by combining satellite and reanalysis soil moisture data. *Hydrol. Earth Syst. Sci.*, **23**, 897–923, <https://doi.org/10.5194/hess-23-897-2019>.
- Zemp, M., and Coauthors, 2015: Historically unprecedented global glacier decline in the early 21st century. *J. Glaciol.*, **61**, 745–762, <https://doi.org/10.3189/2015JoG15J017>.
- , and Coauthors, 2019: Global glacier mass changes and their contributions to sea-level rise from 1961 to 2016. *Nature*, **568**, 382–386, <https://doi.org/10.1038/s41586-019-1071-0>.
- , I. Gärtner-Roer, S. U. Nussbaumer, J. Bannwart, P. Rastner, F. Paul, and M. Hoelzle, Eds., 2020: *Global Glacier Change Bulletin: No. 3 (2016–2017)*. World Glacier Monitoring Service, 274 pp., <https://doi.org/10.5904/wgms-fog-2019-12>.
- Zhang, J., and Coauthors, 2016: Multi-Radar Multi-Sensor (MRMS) quantitative precipitation estimation: Initial operating capabilities. *Bull. Amer. Meteor. Soc.*, **97**, 621–638, <https://doi.org/10.1175/BAMS-D-14-00174.1>.
- Zhang, T., R. G. Barry, K. Knowles, J. A. Heginbottom, and J. Brown, 1999: Statistics and characteristics of permafrost and ground-ice distribution in the Northern Hemisphere. *Polar Geogr.*, **23**, 132–154, <https://doi.org/10.1080/10889379909377670>.
- , J. A. Heginbottom, R. G. Barry, and J. Brown, 2000: Further statistics on the distribution of permafrost and ground ice in the Northern Hemisphere. *Polar Geogr.*, **24**, 126–131, <https://doi.org/10.1080/10889370009377692>.
- Zhang, X., F. W. Zwiers, G. C. Hegerl, F. H. Lambert, N. P. Gillett, S. Solomon, P. A. Stott, and T. Nozawa, 2007: Detection of human influence on twentieth-century precipitation trends. *Nature*, **448**, 461–465, <https://doi.org/10.1038/nature06025>.
- Zhang, Y., and Coauthors, 2016: Multi-decadal trends in global terrestrial evapotranspiration and its components. *Sci. Rep.*, **6**, 19124, <https://doi.org/10.1038/srep19124>.
- , and Coauthors, 2018: A Climate Data Record (CDR) for the global terrestrial water budget: 1984–2010. *Hydrol. Earth Syst. Sci.*, **22**, 241–263, <https://doi.org/10.5194/hess-22-241-2018>.
- Zhou, S., and Coauthors, 2019: Land–atmosphere feedbacks exacerbate concurrent soil drought and atmospheric aridity. *Proc. Natl. Acad. Sci. USA*, **116**, 18848–18853, <https://doi.org/10.1073/pnas.1904955116>.
- , and Coauthors, 2021: Soil moisture–atmosphere feedbacks mitigate declining water availability in drylands. *Nat. Climate Change*, **11**, 38–44, <https://doi.org/10.1038/s41558-020-00945-z>.
- Zhou, Y., A. H. Sawyer, C. H. David, and J. S. Famiglietti, 2019: Fresh submarine groundwater discharge to the near-global coast. *Geophys. Res. Lett.*, **46**, 5855–5863, <https://doi.org/10.1029/2019GL082749>.
- Zika, J. D., N. Skliris, A. T. Blaker, R. Marsh, A. J. G. Nurser, and S. A. Josey, 2018: Improved estimates of water cycle change from ocean salinity: The key role of ocean warming. *Environ. Res. Lett.*, **13**, 074036, <https://doi.org/10.1088/1748-9326/aace42>.